Biochemical Journal 475: 151–168 (2018)
DOI: 10.1042/BCJ20170692

Molecular basis for the integration of environmental signals by FurB from *Anabaena* sp. PCC 7120

Short title: Redox status of *Anabaena* FurB influences zinc binding and FurB-DNA interaction

Violeta C. Sein-Echaluce [1,2], María Carmen Pallarés [3], Anabel Lostao [3,4,5], Inmaculada Yruela [6,7], Adrián Velázquez-Campoy [1,2,4,7,8], M. Luisa Peleato [1,2,7] and María F. Fillat [1,2,7*]

[1]Departamento de Bioquímica y Biología Molecular y Celular, Universidad de Zaragoza, 50009 Zaragoza, Spain. [2]Instituto de Biocomputación y Física de Sistemas Complejos (BIFI), Joint Unit IQFR-CSIC-BIFI, Universidad de Zaragoza, 50018 Zaragoza, Spain. [3]Laboratorio de Microscopías Avanzadas, Instituto de Nanociencia de Aragón (INA), Universidad de Zaragoza, 50018 Zaragoza, Spain. [4] Fundación ARAID, 50018 Zaragoza, Spain. [5] Fundación INA, 50018 Zaragoza, Spain. [6] Estación Experimental de Aula Dei, Consejo Superior de Investigaciones Científicas (EEAD-CSIC), 50059 Zaragoza. [7]GBsC (BIFI, UNIZAR), Unidad Asociada al CSIC. [8] Instituto de Investigación Sanitaria Aragón (IIS Aragon), 50009 Zaragoza, Spain.

* Corresponding author: María F. Fillat. Departamento de Bioquímica y Biología Molecular y Celular. Facultad de Ciencias. Universidad de Zaragoza. Pedro Cerbuna, 12. 50009 Zaragoza, España; Tel. (+34) 976761282; Fax (+34) 976762123. E-mail fillat@unizar.es.

Key words: cyanobacteria, FurB/Zur, zinc homeostasis, redox sensing, heme binding

ABSTRACT

FUR proteins are among the most important families of transcriptional regulators in prokaryotes, often behaving as global regulators. In the cyanobacterium *Anabaena* PCC 7120 FurB (Zur) controls zinc and redox homeostasis through the repression of target genes in a zinc-dependent manner. *In vitro*, nonspecific binding of FurB to DNA elicits protection against oxidative damage and avoids cleavage by DNase I. This study provides for the first time evidence of the influence of redox environment in the interaction of FurB with regulatory zinc and its consequences in FurB-DNA binding affinity. Calorimetry studies showed that, in addition to one structural Zn(II), FurB is able to bind two additional Zn(II) per monomer and demonstrated the implication of cysteine C93 in regulatory Zn(II) coordination. The interaction of FurB with the second regulatory zinc occurred only under reducing conditions. While nonspecific FurB-DNA interaction is Zn(II)-independent, optimal binding of FurB to target promoters required loading of two regulatory zinc ions. Those results combined with site-directed mutagenesis and gel-shift assays evidenced that the redox state of cysteine C93 conditions the binding of the second regulatory Zn(II) and in turn modulates the affinity for a specific DNA target. Furthermore, differential spectroscopy studies showed that cysteine C93 could also be involved in heme coordination by FurB, either as a direct ligand or being located near the binding site. Those results indicate that besides controlling zinc homeostasis, FurB could work as a redox-sensing protein likely modifying its zinc and DNA binding abilities depending on environmental conditions.

ABBREVIATIONS

AFM	Atomic Force Microscopy
CPV	Cysteine-proline-valine motif
DNase I	Deoxyribonuclease I
DTT	Dithiothreitol
EMSA	Electrophoretic Mobility Shift Assay
FUR	Ferric uptake regulator
GdnHCl	Guanidine hydrochloride

ICP-MS	Inductively Coupled Plasma Mass Spectrometry
IPTG	Isopropyl β-D-1-thiogalactopyranoside
ITC	Isothermal Titration Calorimetry
Mur	Manganese uptake regulator
Nur	Nickel uptake regulator
P_{all425}	Promoter region of the *all4725* gene
PAR	4-(2-Pyridylazo)-resorcinol
PDB	Protein Data Bank
P_{furA}	Promoter region of the *furA* gene
PMSF	Phenylmethylsulfonyl fluoride
P_{nifJ}	Promoter region of the *nifJ* gene
Zur	Zinc uptake regulator

INTRODUCTION

The FUR (Ferric uptake regulator) family is a widespread group of prokaryotic transcription factors mainly controlling the homeostasis of metals such as iron (Fur subfamily), zinc (Zur), manganese (Mur) and nickel (Nur). Noteworthy, FUR proteins also intervene in the regulation of peroxide-stress response (PerR) and heme availability (Irr) [1]. *Anabaena* sp. PCC 7120 (hereinafter *Anabaena* sp.) contains three paralogues of the FUR family, namely FurA, FurB and FurC [2]. FurA is a global regulator in cyanobacteria and the main responsible of controlling iron homeostasis [3] and FurC has been proposed to act as a PerR regulator [4]. FurB, the protein under study in this work, acts as a Zur regulator in *Anabaena* sp., controlling zinc homeostasis in a zinc-dependent manner [5]. Also, FurB participates in the control of the oxidative stress response regulating the expression of key antioxidant enzymes [6] and protects DNA against DNase I cleavage and ROS damage *in vitro* [7].

The most extended model for FUR-DNA interaction assumes that FUR proteins generally act as classical repressors, binding in the dimeric form to palindromic A/T-rich sequences at the promoter regions of target genes. Thus, under metal repletion conditions, FUR proteins coordinate the regulatory metal acting as co-repressors and undergo conformational changes that trigger FUR binding to the A/T-rich sequences (FUR-boxes), blocking transcription of target

genes by RNA polymerase [8]. Resolution of the X-ray crystallographic structures from several FUR proteins supports the hypothesis that the binding of the co-repressor metal provokes a local conformational change leading to a pivotal motion of the DNA binding domain with respect to the dimerization domain [9-16]. In some cases, this motion would allow the regulator to acquire a “closed conformation” in which DNA recognition by the two N-terminal domains in the dimer is possible. X-ray structures of FUR proteins such as *Pseudomonas aeruginosa* Fur [9], *Streptomyces coelicolor* Zur and Nur [10, 11], *Vibrio cholerae* Fur [12] and *Escherichia coli* Fur [13] present a closed conformation and have been suggested to present optimal DNA binding. Conversely, structures of *Streptococcus pyogenes* PerR [14], *Helicobacter pylori* Fur [15] and *Mycobacterium tuberculosis* FurB/Zur [16] containing structural and regulatory zinc ions exhibit an open conformation. In these cases, the N-terminal domains are too far from each other to permit optimal interaction with DNA, which likely results in a weaker DNA-protein interaction [17]. As derived from crystallographic studies, metal coordination by FUR proteins affects their DNA binding activity and is therefore an essential aspect to study when characterizing a FUR protein. Typically, FUR proteins contain one structural zinc ion per monomer and a second regulatory metal binding site. However, some of the crystal structures available in the PDB exhibit a third binding site, whose functionality is still under debate. Thus, the location and ligands involved in metal coordination usually help to figure out their function [18]. Most of the FUR proteins known to date contain a structural binding site for zinc (site 1) which normally involves four cysteine residues arranged in CXXC motifs and that is located in the C-terminal domain [10, 11, 14-17, 19, 20]. In all structures, the site present in the region between N- and C-terminal domains is responsible for high-affinity coordination of the regulatory metal and is usually called site 2. Finally, some proteins such as Fur from *H. pylori* [15], FurB/Zur from *M. tuberculosis* [16] and Zur from *S. coelicolor* [11] present a third binding site in the core of the dimerization domain. The function of this site is still controversial; it has been proposed to have a role in dimer formation but it could also work as a second regulatory site, allowing the protein respond to a broader range of metal concentrations.

Apart from coordination of regulatory metals, the ability of FUR proteins to bind DNA can also be modulated by the interaction with other ligands, such as heme. Thus, the interaction of FurA and FurB from *Anabaena* sp. with heme has been shown to inhibit protein activity *in vitro* [7, 21].

Binding of FurA to heme involves cysteine C141 [22]. This residue is part of a CP motif, classically described as a “heme regulatory motif” [23] that is also present in the FurB paralog [7]. The interaction of FurA and FurB with heme would have interesting implications *in vivo* because, under oxidative stress conditions when heme levels increase, they would be released from DNA and would permit transcription of genes involved in the oxidative stress response, such as *dpsA* [24] and *prxA* [25].

Although FurB has been described as a Zur regulator [5], little is known about its zinc binding ability and its influence in the interaction with DNA. With the aim to gain new insights into these processes, we first developed a purification procedure that allowed us obtaining enough pure and active protein for biochemical characterization. Our analyses revealed that recombinant FurB contains one structural zinc ion per monomer and is able to bind up to two additional regulatory zinc ions. Evidences for the consequences of the redox environment of FurB on zinc loading and its affinity for DNA, as well as for the role of C93 in FurB functionality are provided.

EXPERIMENTAL

Bacterial strains and culture conditions

Bacterial strains used in this study are described in Table S1. *E. coli* strains were grown in LB medium at 37ºC with constant shaking of 180 r.p.m. When necessary, medium was supplemented with kanamycin 50 μg ml^{-1}. *Anabaena* sp. was grown at 28ºC in BG-11 medium [26], under illumination of 50 μE m^{-2} s^{-1} and constant shaking of 120 r.p.m.

Protein expression and purification

Anabaena sp. genomic DNA was extracted as previously described [27] and used as a template to amplify the *furB* gene with oligonucleotides all2473N-2 and all2473C (Table S2). The *furB* gene was cloned into NdeI - HindIII restriction sites of a pET-28a(+) plasmid (Novagen), so that FurB protein was expressed with a N-terminal His-tag. A FurB-C93A mutant was obtained with the Quik-Change site directed mutagenesis kit (Stratagene) and oligonucleotides C93A_up and C93A_dw (Table S2). Plasmids were verified by DNA sequencing and transformed into *E. coli* BL21 competent cells for protein overexpression. Cells were grown until the exponential phase and treated with 1 mM IPTG during three hours for optimal protein expression.

For recombinant protein purification, 10 grams of FurB/C93A-overexpressing cells were resuspended in 50 ml of buffer A (0.1 M NaH_2PO_4, 0.01 M Tris, 2 M GdnHCl pH 8) containing 1 mM PMSF. Cells were lysed by ten cycles of sonication at 190 W and the suspension was centrifuged to remove cell debris. The supernatant was loaded into a Chelating Sepharose Fast Flow column (Amersham) that was previously charged with zinc according to manufacturer's conditions. The column was washed with 5 volumes of a solution containing 0.5 M $(NH_4)_2SO_4$ in buffer A. Then, the column was subjected to an additional wash with 35 mM glycine in buffer A until OD_{280} was lower than 0.1. Recombinant proteins were eluted from the column with a linear gradient of 0-1 M imidazole in buffer A. Fractions containing the higher amount of target protein were pooled, dialysed against 10 mM acetic acid/acetate buffer pH 5.5 and stored at -20ºC until use. When necessary, proteins were concentrated with an Amicon Ultra 3K device (Millipore). Proteins were quantified by using the bicinchoninic acid protein assay (Pierce).

PAR staining and ICP-MS assay

The presence of Zn(II) in the protein was verified by PAR staining. 4-(2-Pyridylazo)-resorcinol (PAR) is a reagent that forms an orange-coloured complex with zinc [28]. A denaturing gel containing 5 micrograms of the protein was incubated for five minutes with a solution (20 mM HCl-Tris pH 8, 100 mM NaCl, 5% glycerol) containing 500 µM PAR. 50 mM H_2O_2 was then added to visualize the complex. Zn(II) was quantified by Inductively Coupled Plasma Mass Spectrometry (ICP-MS) at the Servicio de Ionómica from CEBAS-CSIC (Murcia, Spain). For the determination, 22.16 nmol of precipitate-free FurB were scaled up to 10 ml with ICP-grade HNO_3.

Electrophoretic mobility shift assays (EMSA)

Gene promoters were obtained by PCR amplification, using *Anabaena* sp. genomic DNA as a template and with oligonucleotides in Table S2. EMSA assays were performed as previously described [6], using the *all4725* gene promoter as target DNA [5]. To evaluate the influence of heme in the DNA binding ability of the proteins, a 2 µM heme solution in 50 mM Tris-HCl pH 8 was prepared and added to the proteins at 1:5 or 1:10 protein:heme molar ratio.

DNA protection assays

The nonspecific binding of FurB to DNA was analysed by *in vitro* DNA protection assays, with a similar procedure to that described in [7]. FurB (80 pmol) was incubated with 100 ng pUC18

plasmid for 10 minutes at room temperature. Reaction volume was scaled up to 60 µl with a solution of 10 mM BisTris/HCl (pH 7.5), 40 mM KCl, 0.1 mM $MgCl_2$ and 5% (v/v) glycerol. Then, 100 µU of DNase I were added to the sample and incubated for 20 additional minutes. The reaction mixture was divided in two 30 µl samples and proteins were removed from one of them by using the GFX PCR DNA and Gel Band Purification kit (GE Healthcare). As a control, the same experiment was performed with BSA instead of FurB and negative controls (without FurB/BSA) were also included. All samples were analysed by electrophoresis in a 0.8% agarose gel and ethidium bromide staining.

Spectroscopy

Difference spectroscopy was used to study the interaction of FurB/C93A with heme. To prepare heme solutions, 3 micrograms of heme (protoporphyrin IX) were dissolved in 1 ml of 0.1 N NaOH/ethanol (1:9 v/v). The suspension was filtered through a 0.22 µm filter and heme concentration was determined by spectrometry, using the extinction coefficient for heme at 385 nm in 0.1 N NaOH is 58.44 $mM^{-1}\,cm^{-1}$ [29]. From that stock solution, a 2 µM heme solution in 50 mM Tris-HCl pH 8 was prepared. Due to the tendency of heme to dimerize, fresh solutions were prepared for each experiment. Heme solutions were also routinely protected from light. To obtain protein-heme complexes, successive aliquots of a 70 µM protein solution were added into a quartz cuvette containing the 2 µM heme solution and spectra were recorded. To correct volumes, equivalent aliquots of protein buffer (10 mM acetic acid/acetate pH 5.5) were added to the reference cuvette.

Atomic force microscopy (AFM)

Adequate DNA for AFM experiments was constructed as follows: the *all4725* gene promoter was amplified from *Anabaena* sp. genomic DNA using oligonucleotides Pall4725_F, Pall4725_R in Table S2. The PCR product was cloned into a pGEM®-T Easy Vector System (Promega) and the construct was verified by DNA sequencing. To prepare binding reactions, FurB was incubated with 5 ng/µl construct in binding buffer, 10 mM Bis-Tris, 40 mM KCl, 5 mM $MgCl_2$, 0.1 mM $MnCl_2$ with or without 5 µM $ZnSO_4$, pH 7.5 and freshly prepared 2 mM DTT, for 20 minutes at room temperature. Biomolecules were then immobilized on freshly cleaved muscovite mica sheets (Electron Microscopy Sciences). Mica pieces were pretreated with 200 mM $MgCl_2$ for 5

minutes and rinsed with binding buffer prior to biomolecule binding as optimised previously to slightly immobilise DNA strands on such negative surfaces [30]. The concentration of the DNA incubated on the substrates was suitable to get isolated complexes that could be analysed individually.

Images were taken in binding buffer with a Cervantes Fullmode Scanning Probe Microscope (Nanotec Electrónica S.L.). V-shaped silicon nitride cantilevers with integrated pyramidal 2 nm ultrasharp tips exhibiting a spring constant of 0.06 N/m (SNL, Bruker Probes) were used. Jumping mode applying a very low force to work in a repulsive regime was used [31]. Several controls were performed to define the adsorption properties of FurB on naked and pretreated substrate; the effect of FurB concentration on DNA binding; the effect of absence and higher zinc concentrations on binding; and the effect of the protein net charge on binding through incubation of DNA with avidin (Sigma-Aldrich), that has a similar isoelectric point as that of FurB. Image processing was carried out with the WSxM software [32]. Furthermore, each feature or associate was analysed in detail with the zoom function of the program, performed without losing image information and discarding possible artifacts.

Isothermal titration calorimetry (ITC)

FurB/C93A interaction with zinc was analysed with a MicroCal Auto-iTC200 calorimeter (Malvern) at a constant temperature of 20ºC. Protein solutions (FurB and C93A) were used at a final concentration of 20 µM in freshly prepared 10 mM acetic acid/acetate buffer pH 5.5 to avoid protein precipitation. Ligand solution contained 400 µM $ZnSO_4$ in 10 mM acetic acid/acetate buffer pH 5.5. Although this is not a physiological pH, it was selected to avoid the formation of insoluble zinc hydroxides. Extrapolating at neutral pH, a considerable increase in zinc binding affinity is expected. Despite the effect of the pH on the binding affinity, the stoichiometry of binding will not be affected. Protein and ligand solutions were degassed for 2 minutes at 10ºC in a ThermoVac (MicroCal) prior to loading into the system. A sequence of 2-µL injections (0.5 µL/s injection flow) spaced 150 seconds and a stirring speed of 750 rpm were programmed. The dissociation constant was obtained through nonlinear regression of experimental data to a model for either a single ligand binding site or two independent and identical sites, as explained elsewhere [33]. No evidences for more complex models (e.g. non-identical or cooperative binding sites) were observed. When necessary, a reducing agent (DTT)

was added to the solutions at a final concentration of 2 mM. Considerable interaction between DTT and zinc has been reported before, but in our case, DTT has not competitively affected the interaction of zinc with FurB; in fact, the binding affinity for FurB was higher in the presence of DTT. Appropriate controls were performed: calcium-EDTA titrations to calibrate/test the calorimeter, and zinc dilution into buffer in order to evaluate the heat effect associated with that process (heat effects were small and uniform along this dilution experiments, and there was no need to subtract them in the protein-zinc titrations).

Protein modelling

Homology modelling was driven with Modeller [34] using the structures of *H. pylori* Fur (PDB ID: 2XIG) [15], *M. tuberculosis* FurB/Zur (PDB ID: 2O03) [16] and *S. coelicolor* Zur (PDB ID: 3MWM) [11] as templates. Molecular structures and structural models were inspected, analysed and plotted with PyMol 1.4.1 (Schrodinger LLC). The C93 residue in *Anabaena* sp. structural model and the conservative positions in *H. pylori* (P114), *M. tuberculosis* (H98) and *S. coelicolor* (P102) are shown in sticks. Secondary structure prediction was made with PSIPRED [35]. Surface electrostatic potentials were calculated and represented using the PyMol 1.4.1 Program.

RESULTS

FurB purification and assessment of specific and nonspecific DNA binding

In order to study FurB interaction with different ligands, a sufficient amount of pure soluble protein was required. Previous attempts to obtain recombinant FurB with an ionic exchange column followed by metal affinity chromatography [2] or with a heparin column followed by ionic exchange [7] yielded very low protein concentration. Since FUR proteins present a remarkable stability upon chemical denaturation with guanidium chloride [GdnHCl] [36], purification of fully active FUR proteins in the presence of a subdenaturing concentration of this chaotropic agent has been successfully used [37]. In this work, purification of FurB by means of a one-step metal affinity chromatography with Zn(II) in the presence of GdnHCl yielded FurB with purity above 90% (Fig. 1a). Most of the protein was obtained in the monomeric form although, to a much lesser extent, dimers (~34 kDa) could also be observed. After chromatography, FurB was dialyzed in the presence of 10 mM acetic acid/acetate pH 5.5 since it conferred higher protein

stability and resistance to freeze-thawing cycles than other buffers tested. Further attempts to dialyze the protein against higher pH buffers led to protein precipitation.

To confirm proper folding of FurB after dialysis, different experiments were performed to determine the activity of the protein. Those experiments were based on the ability of FurB to bind DNA *in vitro*, both in a specific and in an nonspecific manner, regardless of the purification procedure [7]. Those tests included electrophoretic mobility shift assays, DNA protection assays and atomic force microscopy imaging. As shown in Figure 1b, EMSA assays demonstrated that recombinant FurB was able to recognize and specifically bind the *all4725* gene promoter, a previously described FurB target encoding porphobilinogen synthase [5], leading to the formation of well-defined protein-DNA complexes in the presence of a reducing agent (DTT) and the Zn(II) co-repressor.

Nonspecific binding of FurB to DNA was verified by protection assays, incubating FurB with a pUC18 plasmid and subjecting the mixture to DNase I treatment. The results established that FurB protected DNA because incubation of pUC18 with protein decreased the amount of nicked plasmid upon addition of DNase I (Fig. 1c). In fact, protein bound the DNA so effectively that results could only be easily interpreted when FurB was removed from the sample and plasmid could freely run into the agarose gel.

Apart from EMSA and protection assays, AFM experiments were also performed obtain a deeper insight on both specific and nonspecific binding of FurB to DNA. Figure 2a shows a FurB monomer bound to a single DNA molecule, presumably to the Zur-box of the *all4725* promoter cloned in the pUC18 plasmid (Fig. S1). The size observed for FurB coating DNA, around 6 nm, agrees with previous measurements obtained for FurB (4.0 ± 1 nm) and free DNA (1.5 ± 0.5 nm) on naked mica (Fig. S2). No protein was found unbound to DNA on Mg^{2+} pretreated mica, as can be deduced from the height profiles drawn in the images with DNA. These results were corroborated with those obtained in control measurements scanning FurB on positively charged pretreated mica, in the absence of DNA, where no protein molecules remain bound (not shown). Probably due to the high affinity of FurB for DNA, nonspecific binding of FurB along the plasmid was already observed at protein concentrations around 1-2 nM (Fig. 2b) even in the absence of zinc (Fig. 2c). Hence, it was not possible to observe binding of FurB in the dimeric form that, according to the classical model, is the oligomeric state of FUR proteins acting as transcriptional

regulators. When a higher concentration of regulator was assayed, from 10 to 500 nM, the DNA strand was covered by FurB oligomers of higher degree. This phenomenon was similar in the absence of zinc (Fig. S3) or when zinc concentration was increased (Fig. 2d). Since avidin did not bind to the DNA strands at the working conditions, it can be concluded that the binding interaction is not based just on an electrostatic adsorption (Fig. S2). Furthermore, it should be noted that a previous analysis of FurA-DNA interaction showed still specific binding of FurA to the P_{furA} target at protein concentration as high as 5 μM [30].

Analyses of zinc binding by FurB and its C93A derivative

To get a better understanding of the metalloregulatory properties of FurB, we analysed its zinc content with a PAR staining assay and ICP-MS. Recombinant protein was subjected to SDS-PAGE electrophoresis and the resulting gel was stained with a PAR solution (Fig. S4). The formation of an orange-coloured band evidenced the presence of zinc in FurB and, consequently, an ICP-MS analysis was carried out in order to establish the stoichiometry of zinc ions. Calculations derived from mass spectrometry results determined a content of approximately 1.2 moles of zinc per mole of protein, that is, 1 atom of Zn(II) per monomer. As will be discussed later, the zinc ion detected is likely to be the structural metal that, according to the alignment of FurB with the sequences of FUR proteins from different bacteria, it is probably coordinated by the highly conserved cysteines C81, C84, C121 and C124 (Fig. 3).

Once established that purified FurB contained one zinc ion, the presence of additional binding sites was examined by ITC under reducing and non-reducing conditions (Figs. 4a and 4b). The analysis of the experimental data through nonlinear regression [33], led to the conclusion that in the absence of reducing agent FurB exhibited one binding site with affinity in the micromolar range. However, in the presence of DTT, FurB displayed two binding sites with similar affinities. DTT also increased the binding affinity and made the enthalpy of the interaction less unfavourable (Table 1). The fact that zinc binding was affected by the redox state of FurB led us think about the possible implication of the remaining cysteine residue, C93, in the coordination of one of the regulatory zinc ions. From now on, we will consider regulatory binding sites/ions to those detected by ITC, while the Zn(II) detected by PAR staining and ICP-MS will remain considered structural.

With the aim of studying the potential entanglement of C93 in the coordination of regulatory zinc and therefore in FurB metalloregulation, a C93A mutant was obtained and purified using the same procedure already described for FurB (Fig. 5a). As verified by EMSA assays, the C93A mutant was also active (Fig. 5b). Analogous ITC experiments were carried out with C93A (Figs. 4c and 4d) and data derived from the results are shown in Table 1. As it was observed with FurB, the C93A mutant exhibited only one binding site in the absence of DTT but, conversely, addition of DTT did not lead to the appearance of a second binding site in the mutant. This result supports the hypothesis that C93 could be involved in zinc coordination at one of the regulatory sites. Consequently, substitution of this residue by alanine leads to a decrease in zinc affinity and the detection of only one zinc binding event in the calorimetric experiments under reducing and non-reducing conditions.

In order to confirm whether the location of C93 would be compatible with zinc coordination by this residue, we performed a tridimensional modelling of FurB based on solved X-ray structures of FUR proteins crystallized with three zinc ions: *H. pylori* Fur (Fig. 6a), *M. tuberculosis* FurB/Zur (Fig. 6b) and *S. coelicolor* Zur (Fig. 6c). Interestingly, C93 was located in all FurB models at the beginning of an alpha helix close to a flexible loop. This position could be highly flexible as predicted in particular models from *H. pylori* Fur and *S. coelicolor* Zur allowing C93 to rotate and bind to zinc at site 3 if necessary. The location of C93 at the beginning of an alpha helix in *Anabaena* sp. FurB was also corroborated with the PSIPRED tool for secondary structure prediction (Fig. S5).

Influence of redox status in the specific FurB-DNA interaction

Our previous studies consistently showed that DTT was required for the optimal interaction of FUR proteins with DNA [2, 6]. In order to study the influence of FurB redox state on its interaction with DNA, EMSA assays under different redox conditions were conducted. Figure 7 shows that the presence of DTT substantially favoured and stabilized complex formation (lanes 2 and 3). DTT was also able to partially revert the effect of H_2O_2 on FurB (lanes 4 and 5), as well as in the preformed FurB-DNA complex under oxidizing conditions, clearly indicating that the specific interaction of FurB with DNA is modulated by its redox status.

As previously shown in the EMSA assays with FurB, upon titration of $P_{all4725}$ with the regulator, two clearly defined FurB-DNA complexes could be observed (Fig. 1b). This was in contrast with the smearing obtained when the C93A derivative was incubated with the promoter (Fig. 5b), indicative of complex dissociation along the experiment. Furthermore, the mutant presented a weaker affinity for DNA when compared to FurB (Fig. 5c). Taken altogether, these results indicate that FurB interaction with DNA is redox regulated through C93, since the presence of this residue in the reduced form appears to be necessary for the formation of defined protein-DNA complexes.

Study of FurB/C93A interaction with heme

As previously described, addition of heme to FurB impaired its DNA binding ability, pointing to an interplay between FurB activity and the pool of unbound cellular Fe(II/III) heme [7]. Since FurB contains a putative heme regulatory motif involving C93, EMSA assays in the presence of heme were performed with the C93A mutant as well as with the wild type protein (Fig. 8). Addition of the ligand affected C93A binding to DNA, indicating that both FurB and C93A are able to interact with heme. Due to the high aggregation of FurB in neutral and basic pH buffers, additional controls (lanes C) were performed so as to corroborate that DNA binding was not affected by the buffer in which heme was dissolved (50 mM Tris/HCl pH 8). Hence, the decrease in FurB/C93A DNA binding ability after heme addition was due to the existence of a protein-heme interaction.

Differential spectroscopy experiments were then carried out with the aim of determining the affinity of the protein-heme interaction. Consecutive aliquots of FurB were added to a heme solution and differential spectra were recorded (Fig. 9a). Analogous experiments were performed with C93A to establish whether C93 substitution affected affinity and to infer its implication in heme binding (Fig. 9b). As derived from spectra, both FurB and C93A interacted with heme, exhibiting a shift of the 385 nm band (corresponding to the maximum absorbance of free heme) to approximately 420 nm (maximum absorbance of a protein-heme complex). The $\Delta Abs_{420-385}$ values obtained in both experiments were represented against protein concentration and adjustment to the typical saturation curve of a 1:1 stoichiometry complex was attempted.

Unfortunately, data did not lead to a proper adjustment and affinity constant for the FurB/C93A-heme interaction could not be calculated by this method (not shown).

Determination of the affinity for heme with the ITC technique was also attempted but, again, data obtained did not allow calculation. In this case, ITC results could not be used because either the enthalpy of reaction was too small or there was no interaction under the conditions of the assay. Nevertheless, comparison of both sets of differential spectra shows that the maximum $\Delta Abs_{420-385}$ achieved with C93A was smaller than in the case of FurB, indicating that even though C93 is not essential for heme-FurB interaction, its substitution by an alanine results in a decreased affinity of FurB for heme. The occurrence of C93 either as a direct heme-coordinating amino acid or in its proximal environment was also supported by the presence of two cavities nearby C93 in a protein model based on the average of the structures from *H. pylori* Fur and *M. tuberculosis* Zur (Fig. 9c). In the absence of the zinc ion in site 3, those two potential gateways for heme conformed by C93, H77, H91, H96 and H113, as well as by a hydrophobic pocket surrounded by Q103, F108, F111 and Y113 could certainly contribute to the formation and stabilization of the heme-protein.

DISCUSSION

The proclivity of FUR proteins to form inclusion bodies when recombinantly overexpressed makes its purification challenging. Previous purification procedures yielded low amounts of FurB not suitable for biochemical or structural studies [2, 7]. In this work, we have taken advantage of the high stability of FUR proteins against chemical denaturation using mild concentrations of GdnHCl in the purification procedure to obtain a high yield of active FurB. The presence of GdnHCl has been proposed to decrease interactions favouring protein aggregation and inclusion body formation [37], increasing the yield of the purification process when compared to the previous attempts without denaturing reagent. GdnHCl could also work reducing the nonspecific binding of proteins to the column, allowing for a higher purity of the target protein.

Purified FurB retained its ability to specifically bind DNA *in vitro*, corroborating proper folding of the protein. Recombinant FurB also exhibited the ability to nonspecifically bind and protect DNA against DNase I cleavage. Hence, according to our previous reports [2, 6, 7], the results here

evidence that the nonspecific binding to DNA *in vitro* is an intrinsic ability of FurB, not depending on the purification procedure employed.

Although AFM experiments confirmed the duality in FurB binding to DNA, only protein monomers could be observed specifically bound to DNA. It is noticeable that the presence of protein monomers bound to DNA was also observed in FurA from *Anabaena* sp., which binds the P_{furA} target in a sequential fashion [30]. Unlike FurA, nonspecific binding of FurB to DNA starts by binding of FurB monomers along the DNA chain (Fig. 2b) and only when DNA has been coated, the recruitment of additional FurB molecules to form higher aggregates is observed (Fig. 2d). Notably, nonspecific FurB binding does not require zinc as cofactor (Fig. 2c and Fig. S3). The possible *in vivo* implications of the nonspecific DNA binding ability of FurB have already been discussed [7]. However, further work should be done to identify the environmental factors that trigger massive binding to DNA, as well as the cellular pathways potentially involved in this process.

PAR-staining and ICP-MS analyses indicated that recombinant FurB contained one zinc ion per monomer of protein. PAR staining showed the presence of zinc even under SDS-denaturing conditions, pointing to the structural role of the zinc detected. As previously proposed for other FUR proteins [28], under denaturing conditions, residues involved in structural zinc coordination could form a hairpin-like structure that would allow metal binding (Fig. S4). Thus, we propose that this zinc ion detected in FurB would correspond to the structural one, which in other members of this family is tightly bound to the protein even under denaturing conditions [28, 38].

As already mentioned, structural zinc coordination in FUR proteins usually takes place through the four highly conserved cysteine residues belonging to CXXC motifs in the C-terminal domain [18]. Regarding FurB, there are four residues fulfilling those conditions: C81, C84, C121 and C124. The equivalent cysteines in *B. subtilis* Zur (C95, C98, C132, C135), *S. coelicolor* Zur (C90, C93, C130, C133), *M. tuberculosis* FurB/Zur (C86, C89, C126, C129) and *H. pylori* Fur (C102, C105, C142, C145) are involved in structural zinc coordination [11, 15, 16, 39]. This, together with residue disposition in the different FurB models points to C81, C84, C121 and C124 as ligands to the structural zinc at site 1.

ITC experiments show that, apart from the structural site, reduced FurB presents two additional binding sites with an affinity for zinc in the micromolar range. Intriguingly, in the absence of DTT

FurB exhibited a single regulatory binding site. This indicates that at least one cysteine residue should participate in the coordination of the second regulatory zinc ion, which is only bound to FurB under reducing conditions. Since C81, C84, C121 and C124 are likely involved in structural zinc coordination, C93 would be the only cysteine available. Calorimetry experiments with the C93A mutant supported the hypothesis of C93 being involved in regulatory zinc coordination, because the mutant presented only one regulatory site even under reducing conditions. FurB modelling based on different FUR X-ray crystallographic structures revealed that C93 position would be compatible with regulatory zinc coordination, specifically, at site 3. In all the models used in this work C93 is located in the extreme of an alpha helix and close to flexible regions that would allow residue rotation to coordinate zinc if necessary. A shortening of alpha helix length and a rotation of cysteine binding metal have been observed previously for the apoprotein to metal binding protein transition [40]. Interestingly, a previous bioinformatic analysis based on Zur from *Prochlorococcus marinus* [41] also locates the equivalent to C93 at the sensory site of Zur. Thus, taking all those results into account together with the comparison of EMSA profiles from FurB and the C93 variant, we suggest that FurB activity is influenced by the redox state of C93 that, in turn, determines the loading of the second regulatory zinc ion.

Regarding the other residues involved in zinc coordination at site 3, D75, H77, H96 and H113 occupy equivalent positions to the coordinating residues of site 3 in both *M. tuberculosis* FurB/Zur and *S. coelicolor* Zur [11], so that some of these residues could be implicated in zinc coordination at site 3. Concerning site 2, only H78 is highly conserved among FUR proteins. However, the high proximity between sites 2 and 3, only separated by a flexible loop, would make it possible for residues in the loop (D75 and H77) to intervene in zinc coordination at site 2 instead of site 3. Other residues such as Q21, Q58 and Q73 could also be involved in zinc coordination at site 2. Although coordination through glutamine residues is less frequent [42], metals can interact with the oxygen in the carbonyl group. Another possibility is that the coordination sphere is completed with a water molecule bound to a glutamine residue. This kind of interaction has been found in Fur from *Magnetospirillum gryphiswaldense,* where Q111 is involved in manganese coordination through a water molecule [43]. Only additional mutagenesis studies together with the resolution of the X-ray crystallographic structure of zinc-replete FurB would allow determining residues involved in zinc coordination.

The effect of oxidative stress in zinc uptake, as well as the role of Zur in protecting bacteria from oxidative damage has been established in organisms with very different physiology [6, 44-46]. More recently, an interconnection between FUR proteins and thiol-mediated redox homeostasis has been reported in *B. subtillis*, where Zur and Spx regulons partially overlap [47]. Furthermore, metal and DNA binding of cyanobacterial FurA is controlled by an intramolecular cysteine-based redox switch that integrates iron availability and redox environmental signals [48]. Thus, the integration of metal availability and redox status through redox modulation of cysteine residues could be a feature of cyanobacterial FUR proteins to manage a more precise control of cell homeostasis.

The ability of FurB to bind heme has previously been described [7]. Heme is an essential cofactor and a signal molecule in a source of biological processes. FUR-heme interaction modulates the activity of several members of this family through different mechanisms. While heme binding to Irr triggers protein degradation in rhizobia [49], the interaction of heme with cyanobacterial FurA and FurB results in dampening of protein activity [7, 21]. In *Anabaena* sp., FurA displays the features of a heme-sensor, binding the cofactor through the regulatory motif CP with an affinity in the micromolar range [21, 22]. In a similar way, it was proposed that the CPV motif present in FurB, that contains C93, was involved in FurB-heme interaction. However, further studies were required to verify this hypothesis. Results from the present work show that presence of heme in a 10-fold molar excess severely affected the DNA binding ability of FurB *in vitro*. A similar excess of heme is necessary for inhibition of the activity in other FUR proteins such as FurA from *Anabaena* sp. [21] and Fur from *H. pylori* (Ángela Fernández-Otal, personal communication).

Attempts to calculate the affinity of the FurB-heme interaction by means of differential spectroscopy and ITC were unsuccessful, perhaps due to lability of the interaction. In fact, a common feature of heme-containing proteins with a CPV motif is the transient character of this interaction, essential for an efficient effector-mediated regulation of protein function. Results from differential spectroscopy experiments with C93A, the FurB-derivative with a mutation in the CPV motif, indicated that C93 is likely involved in heme coordination. Whereas differential spectra from the wild type protein presented a clear increase in the absorbance at 420 nm when protein was added to heme, the maximum absorbance at this wavelength was much lower in

C93A. Therefore, as previously suggested in FurA from *Anabaena* sp., where C141 belonging to the CP motif was proposed as an axial ligand for the Fe(III) high-spin heme [22], C93 could be directly involved in heme coordination by FurB. If not directly implicated, C93 could be located in the proximities of the truly binding site, favouring heme recruitment. Histidine residues are usually involved in heme coordination [50] and, hence, it cannot be ruled out that heme binding in FurB could be taking place through some of the histidine residues in close proximity with C93, such as H77, H96 and H113.

Free-heme levels inside the cell increase along with oxidative stress [51], so that the FurB-heme interaction would make sense from a biological point of view. Heme interaction with FurB under oxidative stress would diminish protein affinity for DNA, increasing the transcription of genes such as *sodA* and *alr0998,* which are FurB-regulated and directly involved in the oxidative stress response (Figure 10) [6]. It is also noticeable that *all4725*, whose promoter is used as a positive control in this study because of the high affinity of FurB by its sequence, codes for the porphobilinogen synthase *hemE*, a key enzyme in the heme-synthesis pathway. Interestingly, *all4725* is strongly de-repressed in a Δ*zur* mutant [5], supporting the occurrence of a FurB-heme regulatory interplay.

In summary, our data indicate that *Anabaena* sp. FurB, in addition to controlling zinc homeostasis and the oxidative stress response through direct gene repression, is a redox-responsive protein based on the status of C93 (Fig. 10). This residue seems to play a critical role in FurB activity, contributing to heme recruitment and/or binding and tuning FurB interaction with zinc through its redox state which, in turn, determines the affinity of FurB for DNA. The results reported here establish for the first time a relationship between the redox status of a FUR protein, the functionality of a metal binding site and their contribution to optimal DNA binding. These factors, together with the ability of some FUR paralogs to bind heme conform an additional layer of regulation of these multifunctional proteins.

ACKNOWLEDGEMENTS

Authors would like to thank Drs Andrés González, Ignacio Luque and Teresa Bes for helpful discussion and critical reading of the manuscript. Thanks to Sandra Sampériz for assistance

during protein purification, Dr. Olga Abián for help during ITC data analysis and to Iñigo Echániz and José Luis Diez for technical help.

DECLARATIONS OF INTEREST

Authors declare no conflicts of interest

FUNDING

This work has been supported by grants B18 from Gobierno de Aragón, BFU2012-31458/FEDER & BFU2016-77671-P/FEDER from MINECO and UZ2016-BIO-02 from University of Zaragoza. VCS was recipient of a fellowship from Gobierno de Aragón.

AUTHOR CONTRIBUTION

VCS planned, performed experiments and wrote the manuscript; MCP and AL performed atomic force microscopy experiments; IY performed protein modelling; AV-C analysed ITC results; MLP and MFF planned experiments and wrote the manuscript.

REFERENCES

1 Ma, Z., Jacobsen, F. E. and Giedroc, D. P. (2009) Metal transporters and metal sensors: How coordination chemistry controls bacterial metal homeostasis. Chem. Rev. **109**, 4644-4681

2 Hernandez, J. A., López-Gomollón, S., Bes, M. T., Fillat, M. F. and Peleato, M. L. (2004) Three fur homologues from *Anabaena* sp. PCC7120: exploring reciprocal protein-promoter recognition. FEMS Microbiol. Lett. **236**, 275-282

3 González, A., Bes, M. T., Valladares, A., Peleato, M. L. and Fillat, M. F. (2012) FurA is the master regulator of iron homeostasis and modulates the expression of tetrapyrrole biosynthesis genes in *Anabaena* sp. PCC 7120. Env. Microbiol. **14**, 3175-3187

4 Yingping, F., Lemeille, S., Talla, E., Janicki, A., Denis, Y., Zhang, C.-C. and Latifi, A. (2014) Unravelling the cross-talk between iron starvation and oxidative stress responses highlights

the key role of PerR (alr0957) in peroxide signalling in the cyanobacterium Nostoc PCC 7120. Environ. Microbiol. Rep. **6**, 468-475

5 Napolitano, M., Rubio, M. A., Santamaria-Gomez, J., Olmedo-Verd, E., Robinson, N. J. and Luque, I. (2012) Characterization of the response to zinc deficiency in the cyanobacterium *Anabaena* sp. Strain PCC 7120. J. Bacteriol. **194**, 2426-2436

6 Sein-Echaluce, V. C., González, A., Napolitano, M., Luque, I., Barja, F., Peleato, M. L. and Fillat, M. F. (2015) Zur (FurB) is a key factor in the control of the oxidative stress response in *Anabaena* sp. PCC 7120. Env. Microbiol. **17**, 2006-2017

7 López-Gomollón, S., Sevilla, E., Bes, M. T., Peleato, M. L. and Fillat, María F. (2009) New insights into the role of Fur proteins: FurB (All2473) from *Anabaena* protects DNA and increases cell survival under oxidative stress. Biochem. J. **418**, 201-207

8 Bagg, A. and Neilands, J. B. (1987) Ferric uptake regulation protein acts as a repressor, employing iron (III) as a cofactor to bind the operator of an iron transport operon in *Escherichia coli*. Biochemistry. **26**, 5471-5477

9 Pohl, E., Haller, J. C., Mijovilovich, A., Meyer-Klaucke, W., Garman, E. and Vasil, M. L. (2003) Architecture of a protein central to iron homeostasis: crystal structure and spectroscopic analysis of the ferric uptake regulator. Mol. Microbiol. **47**, 903-915

10 An, Y. J., Ahn, B. E., Han, A. R., Kim, H. M., Chung, K. M., Shin, J. H., Cho, Y. B., Roe, J. H. and Cha, S. S. (2009) Structural basis for the specialization of Nur, a nickel-specific Fur homolog, in metal sensing and DNA recognition. Nucleic Acids Res. **37**, 3442-3451

11 Shin, J. H., Jung, H. J., An, Y. J., Cho, Y. B., Cha, S. S. and Roe, J. H. (2011) Graded expression of zinc-responsive genes through two regulatory zinc-binding sites in Zur. Proc. Natl. Acad. Sci. USA. **108**, 5045-5050

12 Sheikh, A. and Taylor, G. L. (2009) Crystal structure of the *Vibrio cholerae* ferric uptake regulator (Fur) reveals insights into metal co-ordination. Mol. Microbiol. **72**, 1208-1220

13 Pecqueur, L., D'Autreaux, B., Dupuy, J., Nicolet, Y., Jacquamet, L., Brutscher, B., Michaud-Soret, I. and Bersch, B. (2006) Structural changes of *Escherichia coli* Ferric Uptake Regulator during metal-dependent dimerization and activation explored by NMR and X-ray crystallography. J. Biol. Chem. **281**, 21286-21295

14 Makthal, N., Rastegari, S., Sanson, M., Ma, Z., Olsen, R. J., Helmann, J. D., Musser, J. M. and Kumaraswami, M. (2013) Crystal structure of peroxide stress regulator from *Streptococcus pyogenes* provides functional insights into the mechanism of oxidative stress sensing. J. Biol. Chem. **288**, 18311-18324

15 Dian, C., Vitale, S., Leonard, G. A., Bahlawane, C., Fauquant, C., Leduc, D., Muller, C., de Reuse, H., Michaud-Soret, I. and Terradot, L. (2011) The structure of the *Helicobacter pylori* ferric uptake regulator Fur reveals three functional metal binding sites. Mol. Microbiol. **79**, 1260-1275

16 Lucarelli, D., Russo, S., Garman, E., Milano, A., Meyer-Klaucke, W. and Pohl, E. (2007) Crystal structure and function of the zinc uptake regulator FurB from *Mycobacterium tuberculosis*. J. Biol. Chem. **282**, 9914-9922

17 Gilston, B. A., Wang, S., Marcus, M. D., Canalizo-Hernández, M. A., Swindell, E. P., Xue, Y., Mondragón, A. and O'Halloran, T. V. (2014) Structural and mechanistic basis of zinc regulation across the *E. coli* Zur regulon. PLoS Biol. **12**

18 Fillat, M. F. (2014) The FUR (ferric uptake regulator) superfamily: Diversity and versatility of key transcriptional regulators. Arch. Biochem. Biophys. **546**, 41-52

19 Butcher, J., Sarvan, S., Brunzelle, J. S., Couture, J. F. and Stintzi, A. (2012) Structure and regulon of *Campylobacter jejuni* ferric uptake regulator Fur define apo-Fur regulation. Proc. Natl. Acad. Sci. USA. **109**, 10047-10052

20 Traore, D. A. K., El Ghazouani, A., Ilango, S., Dupuy, J., Jacquamet, L., Ferrer, J.-L., Caux-Thang, C., Duarte, V. and Latour, J.-M. (2006) Crystal structure of the apo-PerR-Zn protein from *Bacillus subtilis*. Mol. Microbiol. **61**, 1211-1219

21 Hernandez, J., Peleato, M. L., Fillat, M. F. and Bes, M. T. (2004) Heme binds to and inhibits the DNA-binding activity of the global regulator FurA from *Anabaena* sp. PCC 7120. FEBS Lett. **577**, 35-41

22 Pellicer, S., González, A., Peleato, M. L., Martinez, J. I., Fillat, M. F. and Bes, M. T. (2012) Site-directed mutagenesis and spectral studies suggest a putative role of FurA from *Anabaena* sp. PCC 7120 as a heme sensor protein. FEBS J. **279**, 2231-2246

23 Girvan, H. M. and Munro, A. W. (2013) Heme sensor proteins. J. Biol. Chem. **288**, 13194-13203

24 Hernandez, J. A., Pellicer, S., Huang, L., Peleato, M. L. and Fillat, M. F. (2007) FurA modulates gene expression of alr3808, a DpsA homologue in Nostoc (*Anabaena*) sp. PCC7120. FEBS Lett. **581**, 1351-1356

25 González, A., Bes, M. T., Peleato, M. L. and Fillat, M. F. (2011) Unravelling the regulatory function of FurA in *Anabaena* sp. PCC 7120 through 2-D DIGE proteomic analysis. J. Proteomics. **74**, 660-671

26 Rippka, R., Deruelles, J., Waterbury, J. B., Herdman, M. and Stanier, R. Y. (1979) Generic assignments, strain histories and properties of pure cultures of cyanobacteria. J. Gen. Microbiol. **111**, 1-61

27 Cai, Y. and Wolk, C. P. (1990) Use of a conditionally lethal gene in *Anabaena* sp. Strain PCC 7120 to select for double recombinants and to entrap insertion sequences. J. Bacteriol. **172**, 3138-3145

28 Lee, J.-W. and Helmann, J. D. (2006) Biochemical characterization of the structural Zn2+ site in the *Bacillus subtilis* peroxide sensor PerR. J. Biol. Chem. **281**, 23567-23578

29 Morell, D. B. (1974) Porphyrins and related compounds. In Data for biochemical research (Dawson, R. M., Elliot, D. C., Elliot, W. H. and Jones, K. M., eds.). pp. 314-317, Oxford University Press, Oxford

30 Pallarés, M. C., Marcuello, C., Botello-Morte, L., González, A., Fillat, M. F. and Lostao, A. (2014) Sequential binding of FurA from *Anabaena* sp. PCC 7120 to iron boxes: Exploring regulation at the nanoscale. Biochim. Biophys. Acta. **1844**, 623-631

31 Sotres, J., Lostao, A., Gomez-Moreno, C. and Baro, A. (2007) Jumping mode AFM imaging of biomolecules in the repulsive electrical double layer. Ultramicroscopy. **107**, 1207-1212

32 Horcas, I., Fernández, R., Gómez-Rodríguez, J. M., Colchero, J., Gómez-Herrero, J. and Baro, A. M. (2007) WSXM: A software for scanning probe microscopy and a tool for nanotechnology. Rev. Sci. Instrum. **78**, 013705

33 Vega, S., Abian, O. and Velazquez-Campoy, A. (2015) A unified framework based on the binding polynomial for characterizing biological systems by isothermal titration calorimetry. Methods. **76**, 99-115

34 Sali, A. and Blundell, T. (1993) Comparative protein modelling by satisfaction of spatial restraints. J. Mol. Biol. **234**, 779-815

35 McGuffin, L., Bryson, K. and Jones, D. (2000) The PSIPRED protein structure prediction server. Bioinformatics. **16**, 404-405

36 Hernandez, J. A., Meier, J., Barrera, F. N., de los Paños, O. R., Hurtado-Gómez, E., Bes, M. T., Fillat, M. F., Peleato, M. L., Cavasotto, C. N. and Neira, J. L. (2005) The conformational stability and thermodynamics of Fur A (Ferric Uptake Regulator) from *Anabaena* sp. PCC 7119. Biophys. J. **89**, 4188-4200

37 Pellicer, S., Bes, M. T., González, A., Neira, J. L., Peleato, M. L. and Fillat, M. F. (2010) High-recovery one-step purification of the DNA-binding protein Fur by mild guanidinium chloride treatment. Process Biochem. **45**, 292-296

38 Shin, J.-H. and Helmann, J. D. (2016) Molecular logic of the Zur-regulated zinc deprivation response in *Bacillus subtilis*. Nat. Commun. **7**, 12612

39 Ma, Z., Gabriel, S. E. and Helmann, J. D. (2011) Sequential binding and sensing of Zn(II) by *Bacillus subtilis* Zur. Nucleic Acids Res. **39**, 9130-9138

40 Banci, L., Bertini, I. and Del Conte, R. (2003) Solution structure of apo CopZ from *Bacillus subtilis*: further analysis of the changes associated with the presence of copper. Biochemistry. **42**, 13422-13428

41 Barnett, J. P., Millard, A., Ksibe, A. Z., Scanlan, D. J., Schmid, R. and Blindauer, C. A. (2012) Mining genomes of marine cyanobacteria for elements of zinc homeostasis. Frontiers in Microbiology. **3**, 142

42 Harding, M. M. (2004) The architecture of metal coordination groups in proteins. Acta Crystallogr. D Biol. Crystallogr. **60**, 849-859

43 Deng, Z., Wang, Q., Liu, Z., Zhang, M., Machado, A. C. D., Chiu, T.-P., Feng, C., Zhang, Q., Yu, L., Qi, L., Zheng, J., Wang, X., Huo, X., Qi, X., Li, X., Wu, W., Rohs, R., Li, Y. and Chen, Z. (2015) Mechanistic insights into metal ion activation and operator recognition by the ferric uptake regulator. Nat. Commun. **6**, 7642

44 Scott, C., Rawsthorne, H., Upadhyay, M., Shearman, C. A., Gasson, M. J., Guest, J. R. and Green, J. (2000) Zinc uptake, oxidative stress and the FNR-like proteins of *Lactococcus lactis*. FEMS Microbiol. Lett. **192**, 85-89

45 Gaballa, A. and Helmann, J. D. (2002) A peroxide-induced zinc uptake system plays an important role in protection against oxidative stress in *Bacillus subtilis*. Mol. Microbiol. **45**, 997-1005

46 Smith, K. F., Bibb, L. A., Schmitt, M. P. and Oram, D. M. (2009) Regulation and Activity of a Zinc Uptake Regulator, Zur, in *Corynebacterium diphtheriae*. J. Bacteriol. **191**, 1595-1603

47 Prestel, E., Noirot, P. and Auger, S. (2015) Genome-wide identification of *Bacillus subtilis* Zur-binding sites associated with a Zur box expands its known regulatory network. BMC Microbiology. **15**, 13

48 Botello-Morte, L., Pellicer, S., Sein-Echaluce, V. C., Contreras, L. M., Neira, J. L., Abián, O., Velázquez-Campoy, A., Peleato, M. L., Fillat, M. F. and Bes, M. T. (2016) Cysteine mutational studies provide insight into a thiol-based redox switch mechanism of metal and DNA binding in FurA from *Anabaena* sp. PCC 7120. Antioxid. Redox. Signal. **24**, 173-185

49 Qi, Z., Hamza, I. and O'Brian, M. R. (1999) Heme is an effector molecule for iron-dependent degradation of the bacterial iron response regulator (Irr) protein. Proc. Natl. Acad. Sci. USA. **96**, 13056-13061

50 Schneider, S., Marles-Wright, J., Sharp, K. H. and Paoli, M. (2007) Diversity and conservation of interactions for binding heme in b-type heme proteins. Nat. Prod. Rep. **24**, 621

51 Wegiel, B., Hauser, C. J. and Otterbein, L. E. (2015) Heme as a danger molecule in pathogen recognition. Free Radic. Biol. Med. **89**, 651-661

FIGURE LEGENDS

Figure 1. Purification of FurB and analysis of dual DNA binding. (a) Elution profile during FurB purification analysed by denaturing electrophoresis in 17% polyacrylamide gels. Prior to electrophoresis, samples were precipitated with TCA in order to remove GdnHCl. Each lane contains 15 microliters of aliquot. FurB monomers (M) and dimers (D) are marked with arrows. (b) Gel-shift assays of FurB. *all4725* promoter was used as a specific DNA in all the assays, whereas *nifJ* promoter was used as a competitor. Lane 1 contained free promoters. Lanes 2-8 contained the promoters with FurB at a final concentration of 100, 200, 300, 400, 500, 600 and

700 nM respectively. Optimal conditions (5 μM $ZnSO_4$ and 1 mM DTT) were used in all the assays. The images of the gels were coloured inverted in order to increase the sensitivity of detection. (c) *In vitro* DNA protection assay. Figure shows the 0.8% agarose gel resulting from electrophoresis and arrows indicate nicked (N) and supercoiled (S) plasmid. 100 ng of pUC18 plasmid were used as a substrate and protection against DNase I cleavage was tested. Lane 1: plasmid with no DNase I. Lane 2: plasmid with DNase I. Lane 3: plasmid with FurB (80 pmol) and DNase I. Lane 4: plasmid with BSA (80 pmol) and DNase I. The reactions were incubated and proteins were removed from half of each sample.

Figure 2. Analyses of FurB-DNA interaction by atomic force microscopy. Images correspond to DNA samples incubated with 0.4 nM (a) and 2 nM (b) recombinant FurB in the presence of 5 μM Zn_2SO_4. DNA samples incubated with 2 nM recombinant FurB with no zinc (c) and with 100 μM Zn_2SO_4 (d). All samples contained 5 ng/μl of DNA (pGEM-T with $P_{all4725}$). Right images show DNA trajectories, drawn according to the profiles of the features corresponding with the expected DNA height.

Figure 3. Alignment of a subset of FUR proteins from different bacteria. GenBank accession number for each sequence is: *Anabaena* sp. FurB (WP_010996629), *H. pylori* Fur (O25671), *M. tuberculosis* FurB/Zur (P9WN85), *S. coelicolor* Zur (CAB69729) and *B. subtilis* Zur (NP_390389). Identified and/or potential residues involved in zinc binding sites are highlighted in red (site 1), green (site 2) and blue (site 3) boxes. Alignment was performed with the AlignX tool from Vector NTI software (Invitrogen).

Figure 4. ITC experiments for Zn(II) interacting with FurB/C93A. (a) FurB interaction with zinc in the absence of reducing agent. (b) FurB interaction with zinc in the presence of 2 mM DTT. (c) C93A interaction with zinc in the absence of reducing agent. (d) C93A interaction with zinc in the presence of 2 mM DTT. Figures show the thermograms (thermal power as a function of time) in the upper panels, and the binding isotherms (normalized heat as a function of the ligand/protein molar ratio) in the lower panels.

Figure 5. Purification and specific DNA binding of C93A. (a) Elution profile during purification of the C93A variant analysed by denaturing electrophoresis in 17% polyacrylamide gels. (b) Gel-shift assays of C93A. *all4725* promoter was used as a specific DNA in all the assays, whereas *nifJ* promoter was used as a competitor. Lane 1 contained free promoters. Lanes 2-8 contained the promoters with C93A at a final concentration of 100, 200, 300, 400, 500, 600 and 700 nM respectively. Optimal conditions (5 µM $ZnSO_4$ and 1 mM DTT) were used in all the assays. The images of the gels were coloured inverted in order to increase the sensitivity of detection. (c) Graphical representation of the percentage of remaining free DNA versus FurB (black squares) or C93A concentration (white squares). The curves were adjusted using the Hill equation and are representatives of two different gel shift experiments.

Figure 6. FurB modelling based on the structure of different FUR proteins. Figures show the superposition of *Anabaena* sp. FurB structural models (a, pink; b, grey; c, yellow) and the structure of the corresponding FUR proteins of (a) *H. pylori* PDB ID: 2XIG, magenta); (b) *M. tuberculosis* FurB/Zur (PDB ID: 2O03, blue) and (c) *S. coelicolor* Zur (PDB ID: 3MWM, green). A detail of site 3 is shown on the right side of the figure. The equivalent residues to C93 in each structure are labeled. Structural data of FurB models are available in the Protein Model Database under the codes PM0080730 (*H. pylori*_2xig), PM0080731 (*M. tuberculosis*_2o03) and PM0080732 (*S. coelicolor*_3mwm).

Figure 7. Effect of redox conditions on FurB-DNA interaction. EMSA assays with 250 nM FurB and 5 µM $ZnSO_4$ under different redox status. *all4725* promoter was used as a specific DNA in all the assays, whereas *nifJ* promoter was used as a competitor. Lane 1 contained free promoters. Lane 2: $P_{all4725}$ and P_{nifJ} with FurB. Lane 3: $P_{all4725}$ and P_{nifJ} with FurB and 1 mM DTT. Lane 4: $P_{all4725}$ and P_{nifJ} with FurB and 10 mM H_2O_2. Lane 5: FurB treated with 10 mM H_2O_2 and then with 1 mM DTT previously to incubation with $P_{all4725}$ and P_{nifJ}. Lane 6: FurB-DNA complex challenged with 10 mM H_2O_2. Lane 7: same than lane 6 after addition of 1 mM DTT. Please note that the images of the gels were coloured inverted in order to increase the sensitivity of detection.

Figure 8. EMSA assays in the presence of heme. Lane C- corresponds to the negative control, containing the promoters from genes *all4725* and *nifJ*. Lane C+ is the positive control, with promoters and protein (FurB/C93A) in the optimal binding conditions. Lane C is an additional control containing promoters, protein and an aliquot of the buffer for heme dissolution (50 mM TRIS/HCl pH 8). Lanes 1:5 and 1:10 contain the indicated protein:heme proportion. Optimal binding conditions were used in all cases (5 μM $ZnSO_4$ and 1 mM DTT) and proteins were added at a final concentration of 500 nM. Note that the images of the gels were coloured inverted in order to increase the sensitivity of detection.

Figure 9. Interaction of FurB and C93A with heme. Differential spectra of heme bound to FurB (a) and C93A (b). Protein (FurB/C93A) was added to a 2 μM heme solution and spectra were recorded. Final protein concentration in each experiment is indicated in the legend. Included spectra are: blank (0 μM protein), intermediate protein additions and the addition of protein leading to the highest $\Delta Abs_{420-385}$ value. (c) Model of the C93 environment in FurB. Simulations of surface electrostatic potential distribution were performed using the FurB model based on the average of the structures from *H. pylori* Fur (PDB ID: 2XIG) and *M. tuberculosis* Zur (PDB ID: 2O03). The open cavities in the absence of zinc are indicated with arrows. Positively and negatively charged regions are depicted in blue and red, respectively.

Figure 10. Role of C93 in the relationship between oxidative stress, ligand binding and the regulation of target genes by FurB. (a) Under reducing conditions and zinc repletion C93 is reduced, FurB binds both regulatory zinc ions and displays high affinity for its DNA targets repressing their transcription. (b) Oxidative or nitrosative stresses led to the oxidation of C93 and the release of a regulatory zinc ion along with the increase of free heme in the cell. Under these conditions the affinity of FurB for its target genes decreases, allowing their transcription. Thus, the oxidation state of C93 tunes the binding of the second regulatory zinc by FurB that is required for optimal DNA-binding. C93 also contributes to heme recruitment, modulating FurB-DNA interaction.

TABLES

Table 1. Parameters estimated by ITC for the interaction of FurB/C93A with Zn(II). n refers to the number of binding sites.

Sample	K (M^{-1})	K_d (μM)	ΔH (kcal/mol)	n
FurB	$2.9 \cdot 10^4$	35.0	6.3	0.99
FurB + DTT	$1.5 \cdot 10^5$	6.5	0.7	2.20
C93A	$4.7 \cdot 10^4$	21.0	5.0	0.93
C93A + DTT	$1.3 \cdot 10^5$	7.8	0.8	0.90

SUPPLEMENTARY MATERIAL

Table S1. Bacterial strains used in this study

Strains	Characteristics and use	Source
E. coli DH5α	F- ϕ80*lac*ZΔM15Δ(*lac*ZYA-*arg*F)U169 *rec*A1 *end*A1 *hsd*R17(rK-, mK+) *pho*A *sup*E44 *thi*-1 *gyr*A96 *rel*A1 λ- Plasmid conservation	Invitrogen
E. coli BL21	F– *omp*T *hsd*SB(*r*B-, *m*B-) *gal dcm* Protein overexpression	Invitrogen
Anabaena sp. PCC 7120	Wild type	Pasteur Institute, Paris, France

Table S2. Oligonucleotides used in this study

Name	Sequence (5'→3)	Purpose
all2473N-2	GGAATTCCATATGAGAGCCATACGC	*furB* cloning in pET-28a (+)
all2473C	CAGTAGTTTAAGCTTTTGACTA	
C93A_up	GTGTATCTATTCCTATTCATCAAGCCCCTG TTCACAACTTAGAAGAAC	Site directed mutagenesis
C93A_dw	GTTCTTCTAAGTTGTGAACAGGGGCTTGAT GAATAGGAATAGATACAC	
PnifJ_up	GCCTACTCTGCGAGTTCTCCG	EMSA *nifJ* promoter
PnifJ_dw	GGCCTGTGAGAGTTGCTGCAC	
Pall4725_F	CTCCGGTGGCACAGGTATTGGC	EMSA *all4725* promoter and cloning in pGEM-T
Pall4725_R	CAGTGTTGCAGTCCGACGCAACCG	

Figure S1. Sequence of the *all4725* gene. The coding sequence is highlighted in grey. The forward and reverse primers used for the amplification of the promoter region are depicted in bold letters. The Zur-box is underlined.

Figure S2. Protein and DNA controls for atomic force microscopy imaging. (a) Representative images of FurB bound to naked mica. (b) 100 ng/μl DNA construct incubated on mica pretreated with 500 mM $MgCl_2$. Mg^{2+} reduces the natural repulsion between negatively charged DNA and mica. The excess of Mg in the treatment of mica makes the strands remain strongly attached to the surface composing higher structures. (c) 1 μM avidin incubated with 5 ng/μl DNA construct scanned in binding buffer without zinc. No protein appears bound to the DNA. At this Mg^{2+} concentration used in the pretreatment, DNA molecules remain attached only by some points leaving some parts free to move in the fluid; that is the reason why DNA strands appear diffuse at the images. The area corresponds to 500 nm^2.

Figure S3. Effect of FurB concentration on binding to DNA by atomic force microscopy. AFM maximum contrast images showing representative FurB-DNA samples in absence of zinc. The concentration of the DNA construct remained constant at 5 ng/μl while FurB concentration increases from (a) 0.5, (b) 1, (c) 2.5 to (d) 5 μM. The higher FurB ratio induces the higher protein density bound to DNA in the images. The scales are omitted for clarity.

Figure S4. Zinc detection and quantification in FurB. (a) Coomassie Blue stained SDS-PAGE gel. Lane 1: molecular markers; lane 2: purified recombinant FurB (left) and a twin gel stained with PAR (right). (b) Schematic representation of FurB under denaturing conditions. Residues proposed to be binding structural zinc are labeled.

Figure S5. Secondary structure prediction of FurB from *Anabaena* sp. Prediction obtained with PSIPRED tool (http://bioinf.cs.ucl.ac.uk/psipred/).

Figure 1

(a)

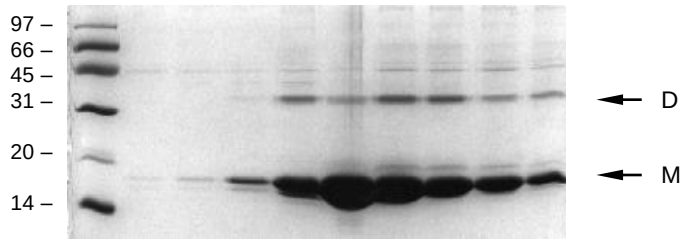
97 –
66 –
45 –
31 –
20 –
14 –
D
M

(b)

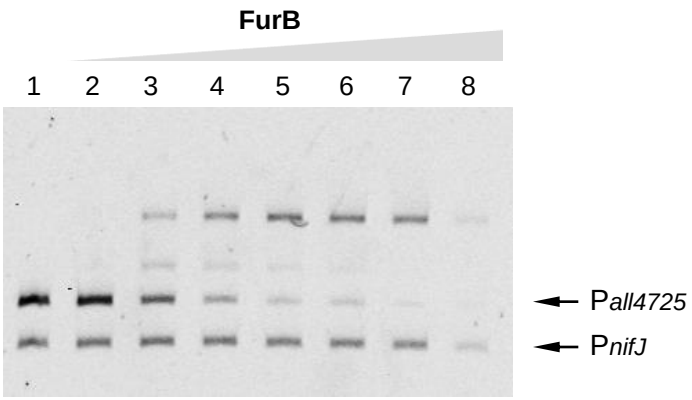
FurB
1 2 3 4 5 6 7 8
Pall4725
PnifJ

(c)

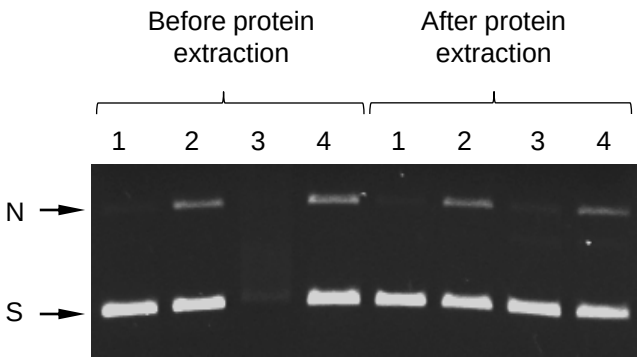
Before protein extraction
After protein extraction
1 2 3 4 1 2 3 4
N
S

Figure 2

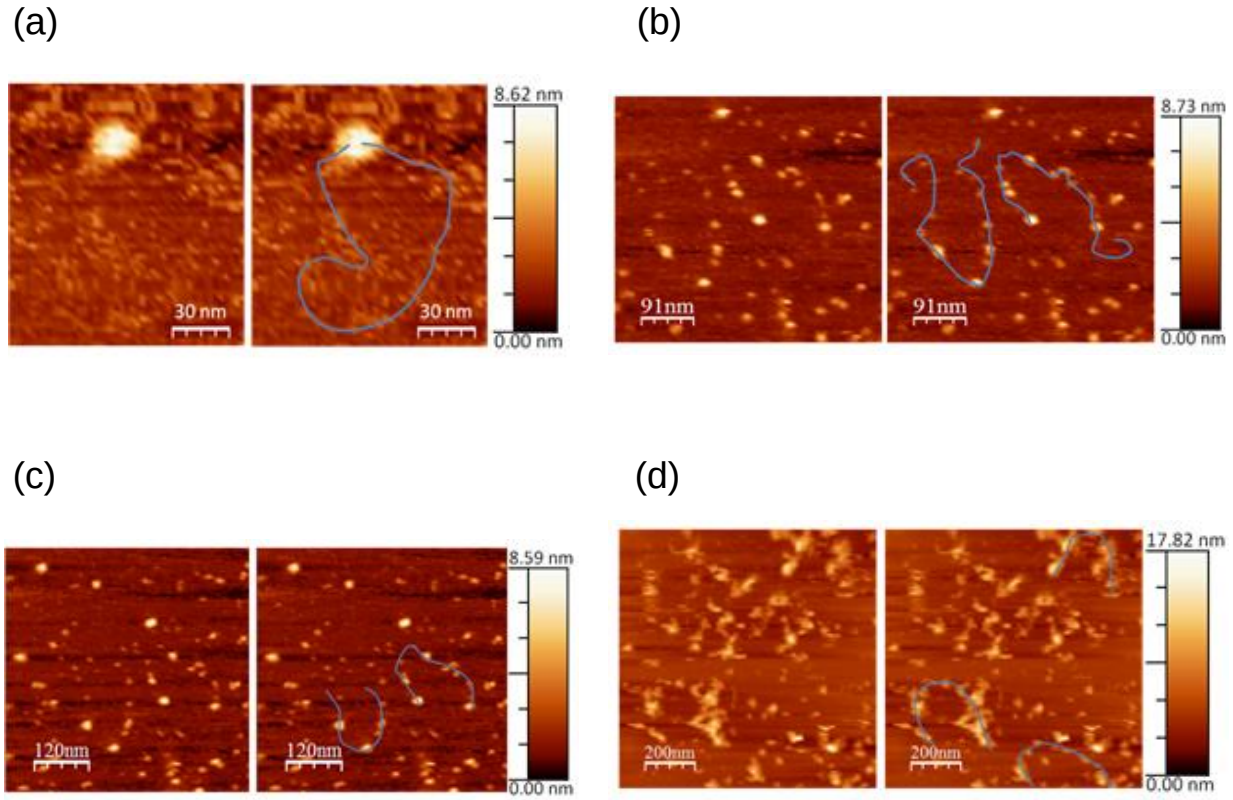
(a)
8.62 nm
30 nm
30 nm
0.00 nm
(b)
8.73 nm
91nm
91nm
0.00 nm
(c)
8.59 nm
120nm
120nm
0.00 nm
(d)
17.82 nm
200nm
200nm
0.00 nm

Figure 3

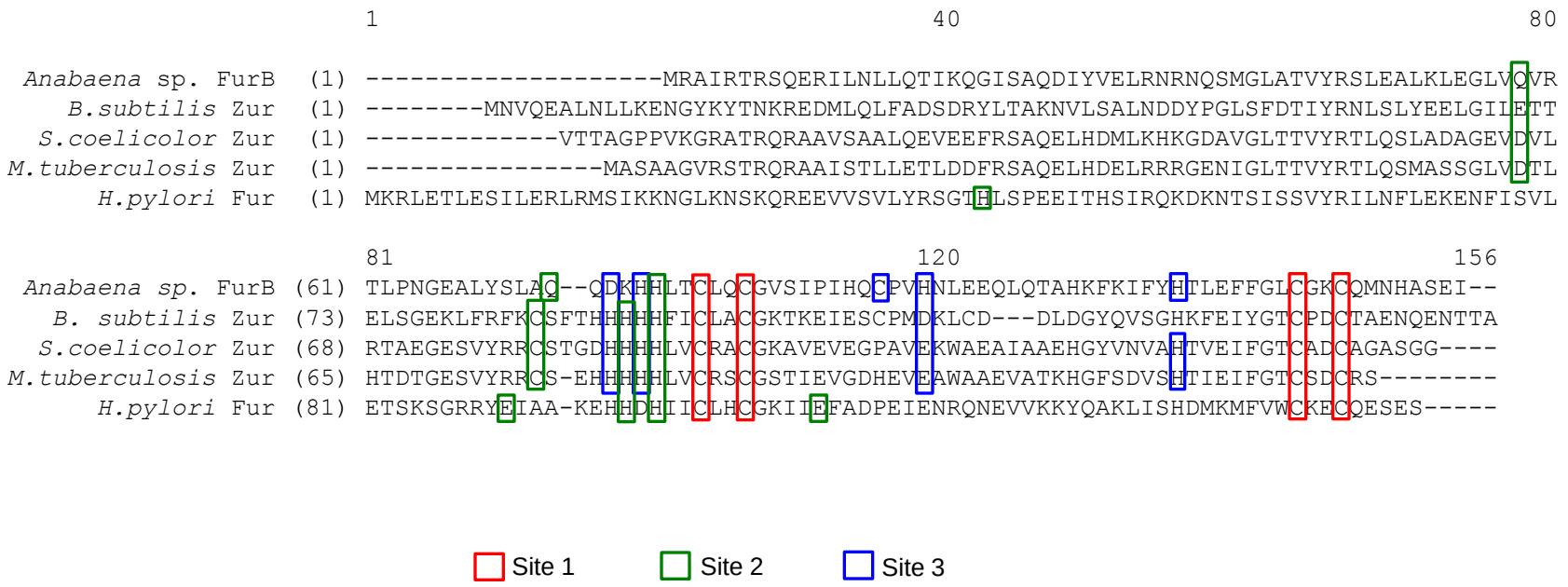
1
40
80
Anabaena sp. FurB (1) ----------MRAIRTRSQERILNLLQTIKQGISAQDIYVELRNRNQSMGLATVYRSLEALKLEGLVQVR
B.subtilis Zur (1) --------MNVQEALNLLKENGYKYTNKREDMLQLFADSDRYLTAKNVLSALNDDYPGLSFDTIYRNLSLYEELGIIETT
S.coelicolor Zur (1) ----------VTTAGPPVKGRATRQRAAVSAALQEVEEFRSAQELHDMLKHKGDAVGLTTVYRTLQSLADAGEVDVL
M.tuberculosis Zur (1) ----------MASAAGVRSTRQRAAISTLLETLDDFRSAQELHDELRRRGENIGLTTVYRTLQSMASSGLVDTL
H.pylori Fur (1) MKRLETLESILERLRMSIKKNGLKNSKQREEVVSVLYRSGTHLSPEEITHSIRQKDKNTSISSVYRILNFLEKENFISVL
81
120
156
Anabaena sp. FurB (61) TLPNGEALYSLAQ--QDKHHLTCLQCGVSIPIHQCPVHNLEEQLQTAHKFKIFYHTLEFFGLCGKCQMNHASEI--
B. subtilis Zur (73) ELSGEKLFRFKCSFTHHHHHFICLACGKTKEIESCPMDKLCD---DLDGYQVSGHKFEIYGTCPDCTAENQENTTA
S.coelicolor Zur (68) RTAEGESVYRRCSTGDHHHHLVCRACGKAVEVEGPAVEKWAEAIAAEHGYVNVAHTVEIFGTCADCAGASGG----
M.tuberculosis Zur (65) HTDTGESVYRRCS-EHHHHHLVCRSCGSTIEVGDHEVEAWAAEVATKHGFSDVSHTIEIFGTCSDCRS--------
H.pylori Fur (81) ETSKSGRRYFIAA-KEHHDHIICLHCGKIIEFADPEIENRQNEVVKKYQAKLISHDMKMFVWCKECQESES-----
Site 1
Site 2
Site 3

Figure 4

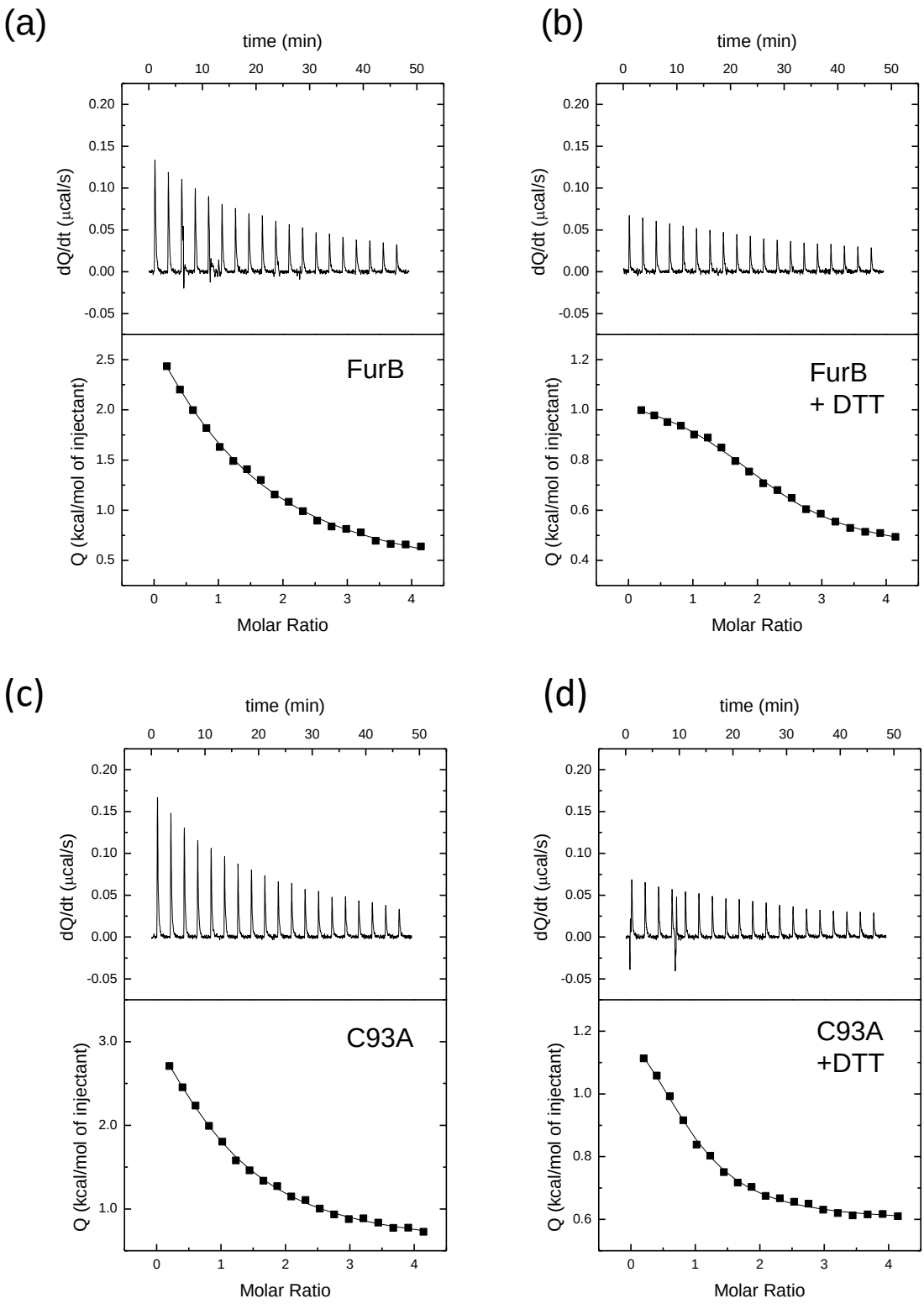
(a)
time (min)
dQ/dt (μcal/s)
Q (kcal/mol of injectant)
FurB
Molar Ratio
(b)
time (min)
dQ/dt (μcal/s)
Q (kcal/mol of injectant)
FurB
+ DTT
Molar Ratio
(c)
time (min)
dQ/dt (μcal/s)
Q (kcal/mol of injectant)
C93A
Molar Ratio
(d)
time (min)
dQ/dt (μcal/s)
Q (kcal/mol of injectant)
C93A
+DTT
Molar Ratio

Figure 5

(a)

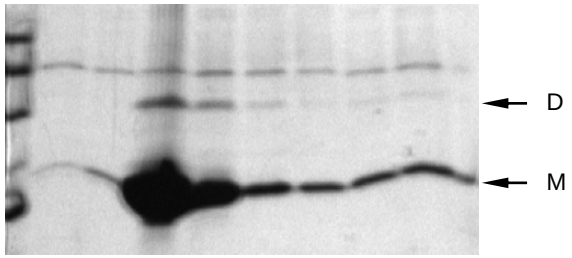

(b)

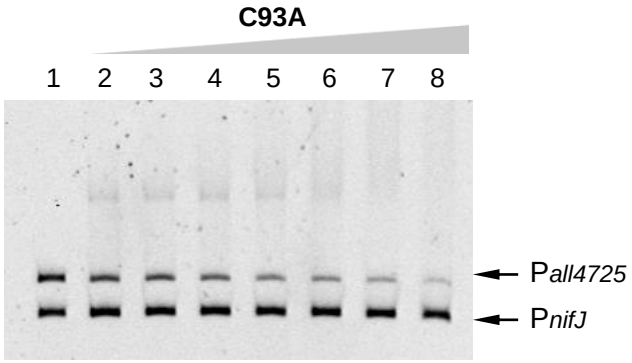

(c)

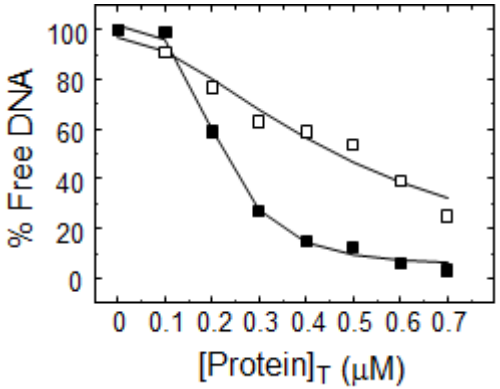

Protein	K_d (nM)
FurB	220± 10
C93A	500± 60

Figure 6

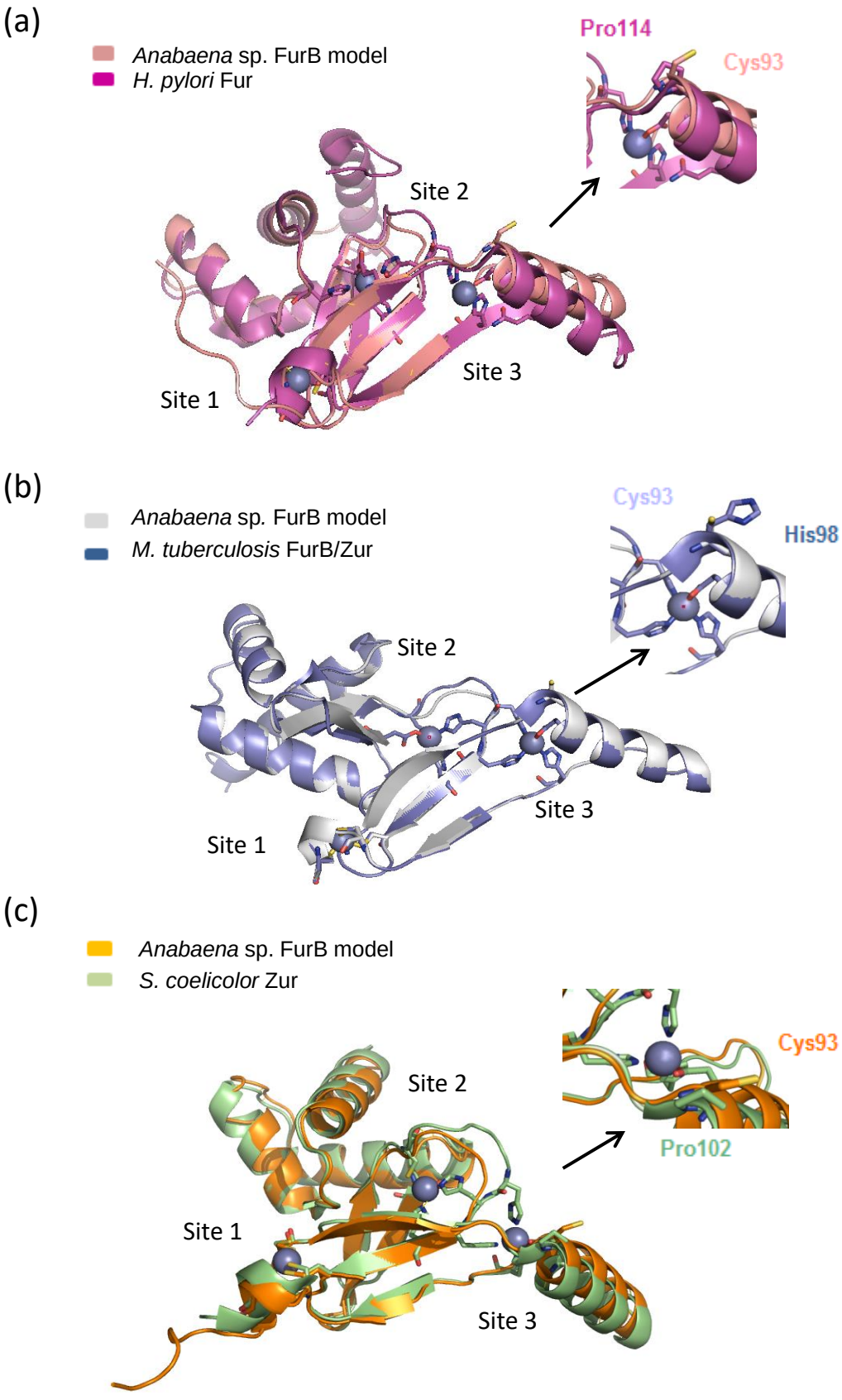
(a)
Anabaena sp. FurB model
H. pylori Fur
Pro114
Cys93
Site 2
Site 3
Site 1
(b)
Anabaena sp. FurB model
M. tuberculosis FurB/Zur
Cys93
His98
Site 2
Site 3
Site 1
(c)
Anabaena sp. FurB model
S. coelicolor Zur
Cys93
Pro102
Site 2
Site 1
Site 3

Figure 7

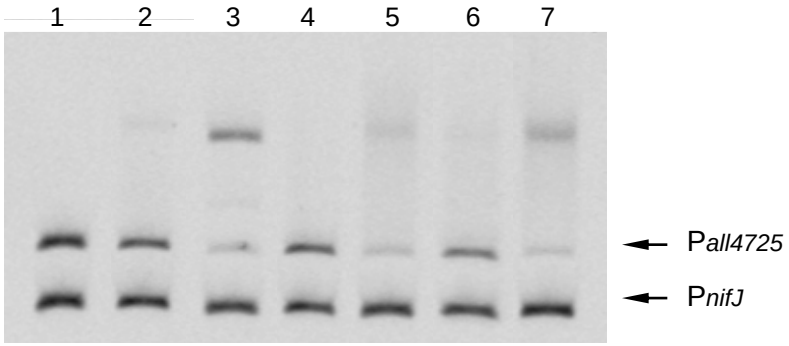

Figure 8

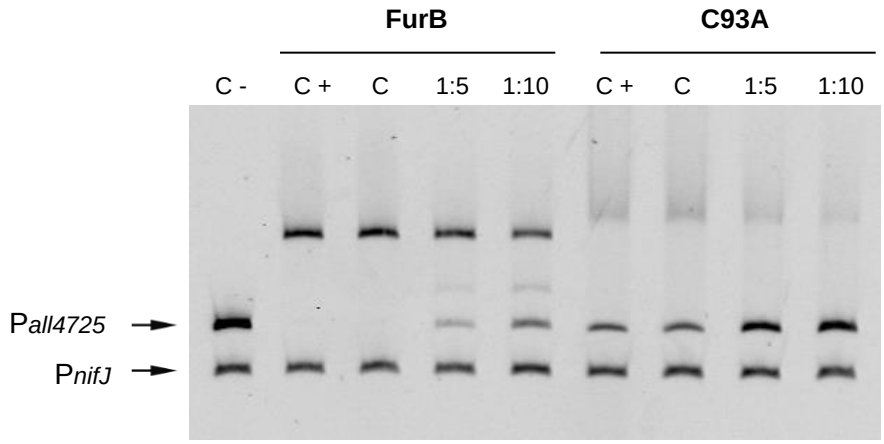

Figure 9

(a)

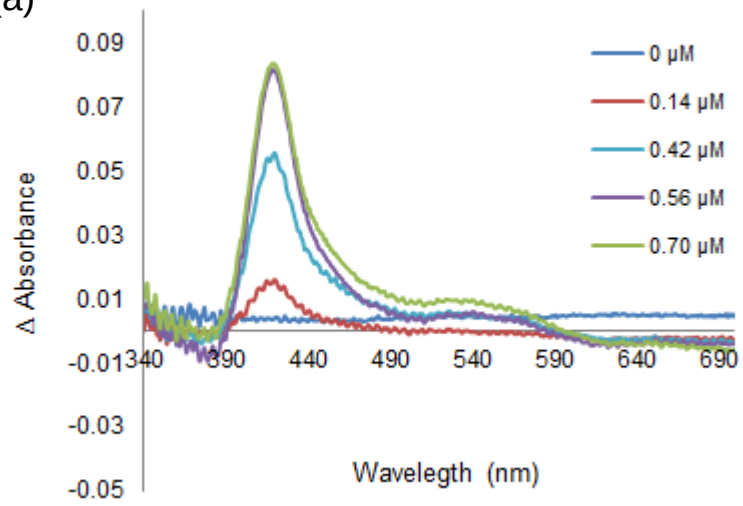
0.09
0.07
0.05
0.03
0.01
-0.01
-0.03
-0.05
Δ Absorbance
340
390
440
490
540
590
640
690
Wavelegth (nm)
0 μM
0.14 μM
0.42 μM
0.56 μM
0.70 μM

(b)

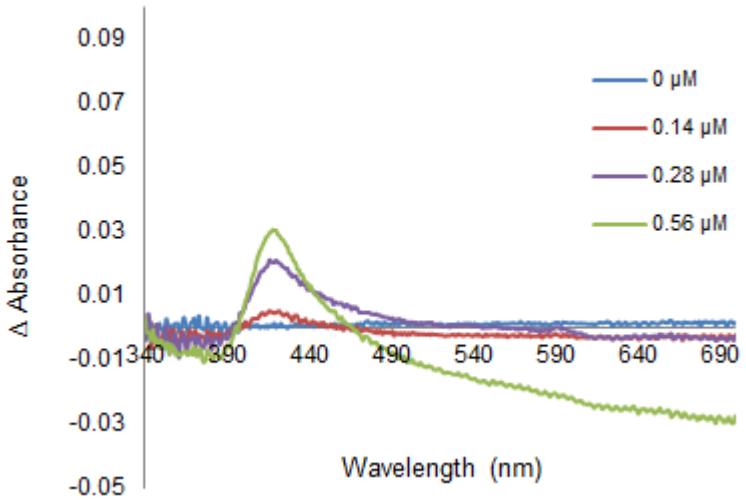
0.09
0.07
0.05
0.03
0.01
-0.01
-0.03
-0.05
Δ Absorbance
340
390
440
490
540
590
640
690
Wavelength (nm)
0 μM
0.14 μM
0.28 μM
0.56 μM

(c)

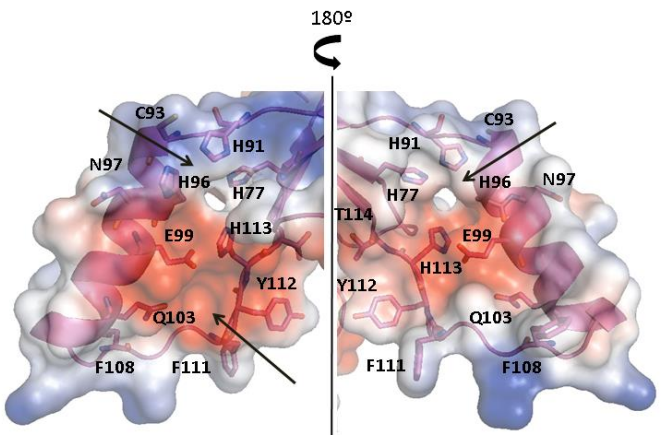
180º
C93
H91
N97
H96
H77
E99
H113
Y112
Q103
F108
F111
T114

Figure 10

(a)

Zn^{2+} repletion and reducing conditions

- Reduced C93
- Loading of both regulatory Zn^{2+}
- Optimal FurB-DNA interaction

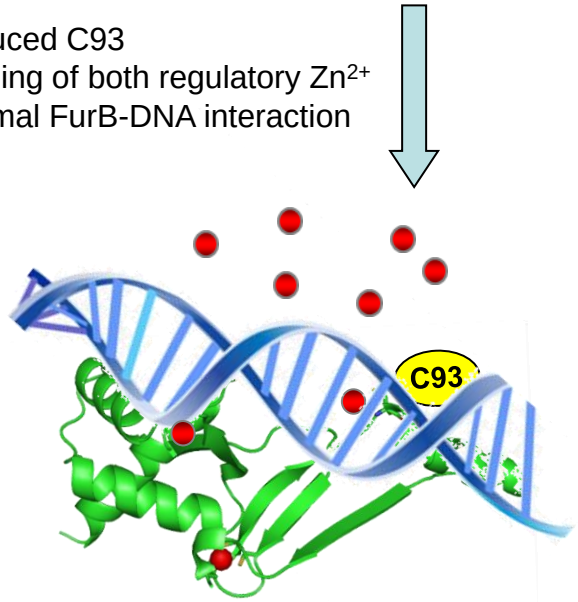

Repression of target genes

(b)

ROS
NOS

Free heme increases

Release of zinc from site 3

Heme interacts with FurB in the vicinity of C93

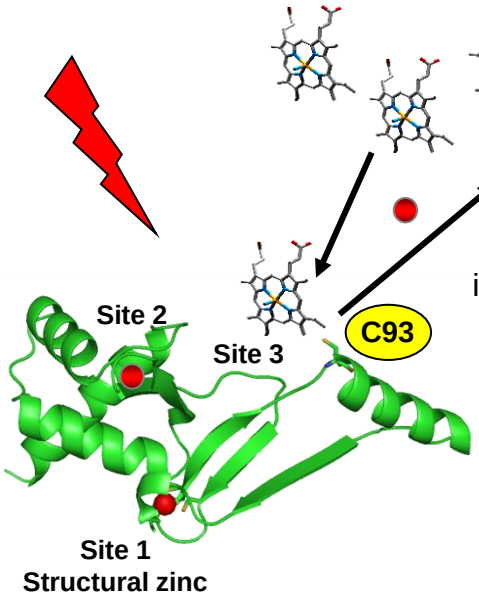

Binding of FurB to DNA decreases

Transcription of target genes

Figure S1

CTCCGGTGGCACAGGTATTGGCTTAACTATCACTAAACACCTAGTAGAACTACAAAGTGGCGAA
ATTCATCTAGATAGTGAACTAGGTATTGGCAGCACGTTCCGCTTTTGTTTGCCTTTAGCATAAG
CACGAGTTCATAGATCCCCGACTTTTTAAAAAAGTCGGGGATCTGAGCGTTCCTACAACACAAA
ATGAACGGCTTCCATTATGATAATGGTTATCAATCTTGTGAAGTCTTTGAAGTCTTATGTCAGT
TGAAAATTCATCTACCGCCAAACCATTGAACCTGTTGCAACGCCCCCGT**CGGTTGCGTCGGACT**
GCAACACTGAGGCGGATGGTGCGGGAAACTACCCTGACAGTGGATGATTTGATTTATCCGATGT
TTGTCATGGAAGGAGAGGGGCAGAAAGTAGAAATTACTTCCATGCCAGGATGTTATCGCTACTC
CCTAGATTTGTTGCTCAAAGAGATAGCCGAAGTATCACAGCTAGGAATTCCGGCGATCGCACTT
TTCCCTGTCATCTCCGAAAATAAGAAAGATGACATCGGTGCAGAAAGCTACAACCCAGAGGGAT
TAGTACAGCAAACAGTCAAAGCCATTAAACAAGCAGTTCCCGATATTGTTGTGATCACTGACGT
AGCCCTTGACCCCTTCACCACACATGGACACGATGGTTTAGTTGATGAAAACGGCACAATCTTA
AATGACCCCACAGTGGAAATGTTAGTGAAAATGGCACTTTCCCAAGCCGCCGCCGGTACAGATT
TTGTTGCCCCTTCCGACATGATGGACGGCAGAATTGGCGCAATCCGTCAAGCCTTAGATGCAGA
AGGCTACATCAATGTAGGGATTTTGGCATACTCCGCTAAATACGCCTCCGCCTATTACGGCCCC
TTTCGGGATGCGTTAGATTCCGCCCCCAAATTTGGCGACAAAAAAACCTATCAAATGGATGCAG
CCAACGCCAGAGAAGCAATTAAAGAAGTAGAACTAGATATTGTCGAAGGTGCAGATATTGTTAT
GGTAAAACCTGCCCTAGCTTACCTAGATATCATTCATCAAGTCCAGCAAGCTACCCAGTTACCA
GTTGCAGCCTACAACGTCAGTGGCGAATACGCCATGATCAAAGCTGCGGCTCAAATGGGTTGGA
TTAATGAAAAACAAGTGATTTTGGAATCTTTAACCAGCATGAAACGCGCCGGCGCAGATTTAAT
TCTCACCTACTTTGCCAAAGAAGTAGCACTGATGTTGCTTTAG

Figure S2

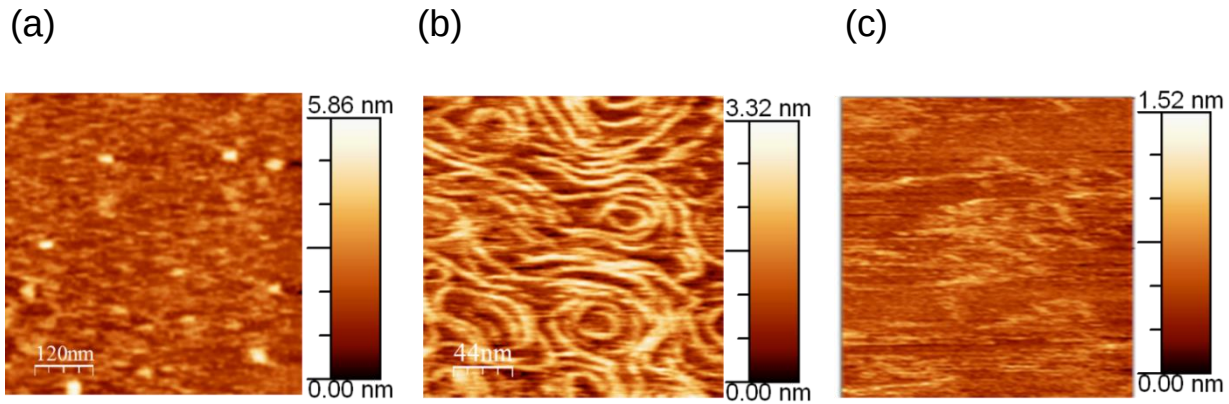

Figure S3

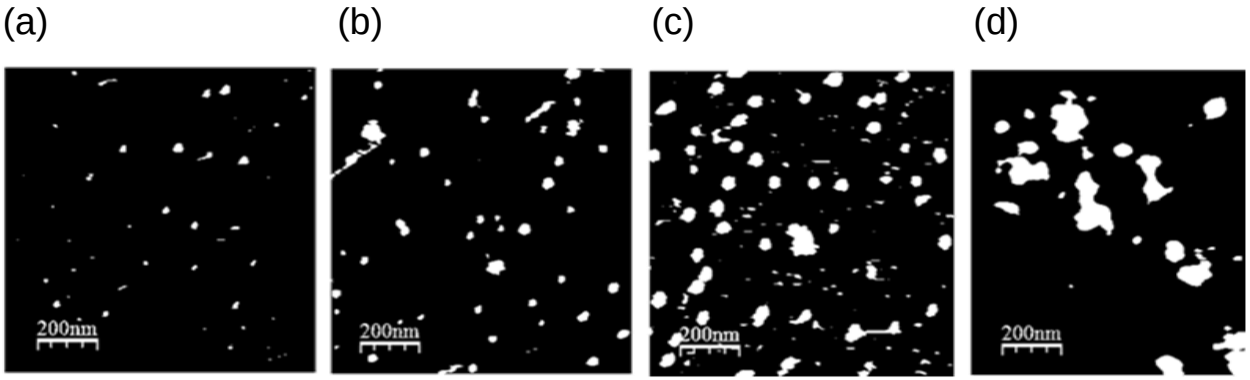

Figure S4

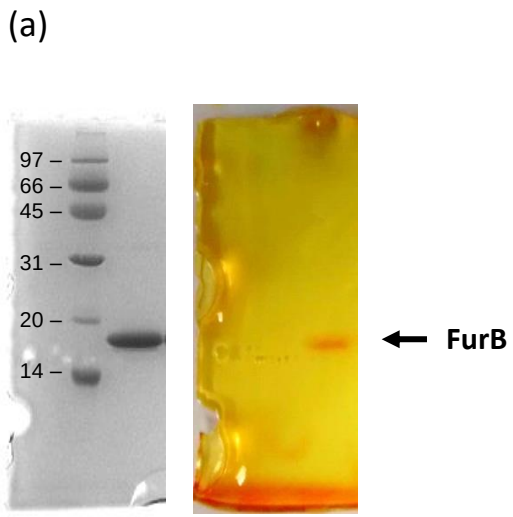

Figure S5

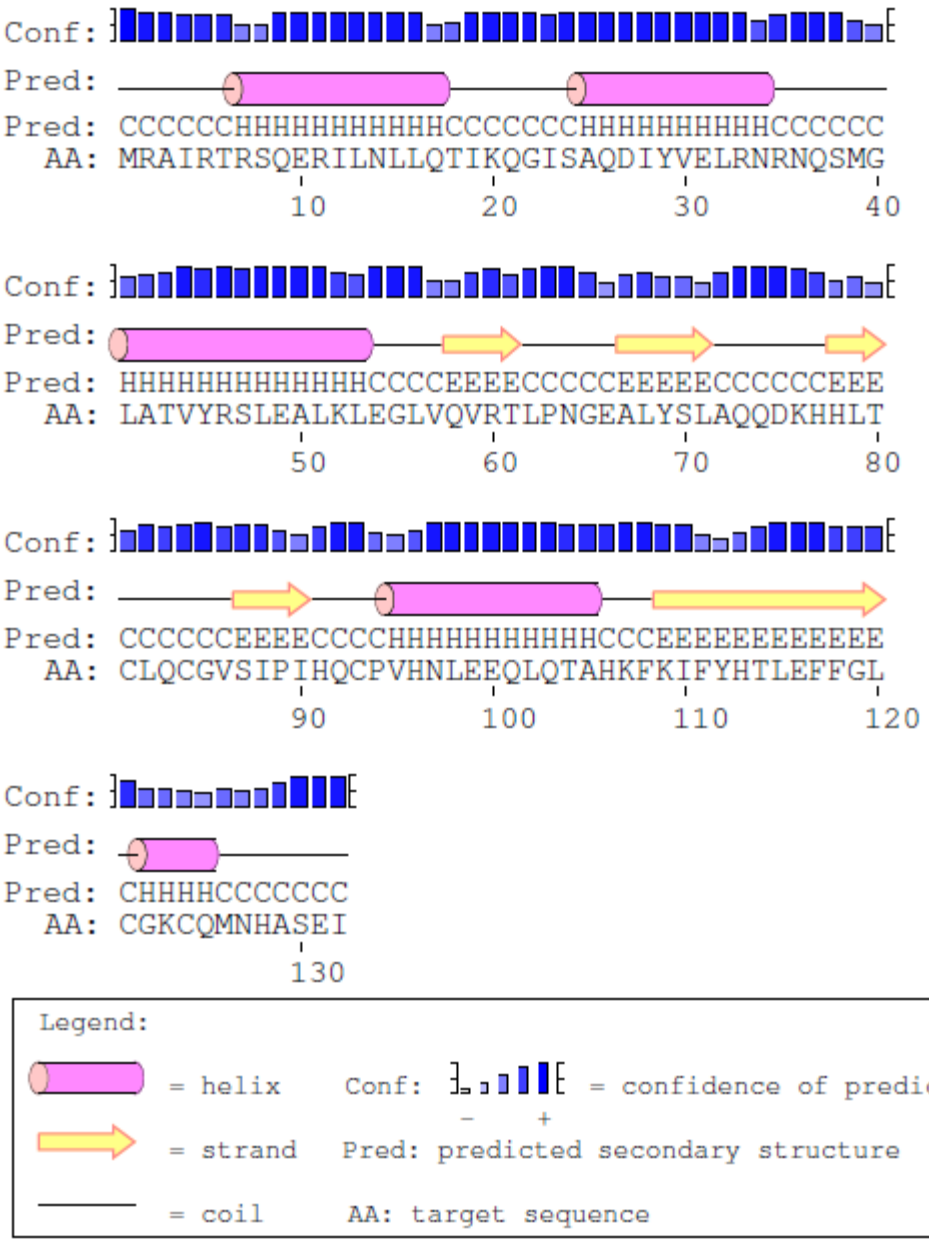
Conf:
Pred:
Pred: CCCCCCHHHHHHHHHHHCCCCCCCHHHHHHHHHHCCCCCC
AA: MRAIRTRSQERILNLLQTIKQGISAQDIYVELRNRNQSMG
10
20
30
40
Conf:
Pred:
Pred: HHHHHHHHHHHHHCCCCEEEECCCCCEEEEECCCCCCEEE
AA: LATVYRSLEALKLEGLVQVRTLPNGEALYSLAQQDKHHLT
50
60
70
80
Conf:
Pred:
Pred: CCCCCCEEEECCCCHHHHHHHHHHHCCCEEEEEEEEEEE
AA: CLQCGVSIPIHQCPVHNLEEQLQTAHKFKIFYHTLEFFGL
90
100
110
120
Conf:
Pred:
Pred: CHHHHCCCCCCC
AA: CGKCQMNHASEI
130
Legend:
= helix
= strand
= coil
Conf:
= confidence of prediction
Pred: predicted secondary structure
AA: target sequence